SIAM J. SCI. COMPUT.
Vol. 14, No. 5, pp. 1107–1142, September 1993
© 1993 Society for Industrial and Applied Mathematics
007

# HIGH-ORDER AND EFFICIENT METHODS FOR THE VORTICITY FORMULATION OF THE EULER EQUATIONS*

J. S. LOWENGRUB†, M. J. SHELLEY‡, AND B. MERRIMAN§

**Abstract.** In this work, the authors develop new methods for the accurate and efficient solution of the two-dimensional, incompressible Euler equations in the vorticity form. Here, the velocity is recovered directly from the Biot–Savart relation with vorticity, and the vorticity is evolved through its transport equation. Using a generalized Poisson summation formula, the full asymptotic error expansion is constructed for the second-order point vortex approximation to the Biot–Savart integral over a rectangular grid. The expansion is in powers of $h^2$, and its coefficients depend linearly upon only local derivatives of the vorticity. In particular, the second-order term depends only upon the vorticity gradient. Except at second-order, the coefficients also involve rapidly convergent, two-dimensional lattice sums. At second-order, the sum is conditionally convergent, but can be calculated easily and rapidly. Therefore, we can remove the second-order term explicitly from the point vortex approximation to obtain a fourth-order discretization. In the special case of a square grid, the second-order error term is orthogonal to the vorticity gradient. The convective derivative of vorticity is thus calculated to fourth order using the unmodified point vortex approximation and automatically yields a fourth-order evolution. These methods have been implemented. For the vorticity transport equation, the point vortex sums are evaluated very rapidly using the fast Fourier transform (FFT) algorithm, and vorticity gradients are approximated using high-order difference methods. With high resolution, the authors solve numerically the roll-up of a thin layer of vorticity through the Kelvin–Helmholtz instability, and the interaction of two oppositely signed vortices driven together under an external strain flow. In the latter case, a simple time dependence of the grid is introduced to maintain resolution of the flow.

**Key words.** vorticity formulation, Biot–Savart integral, point vortex discretization

**AMS subject classifications.** primary 65M25; secondary 76C05

## 1. Introduction.

In this work, we develop and test new methods for the accurate and efficient solution of the two-dimensional, incompressible Euler equations in the vorticity form. Here, the velocity is recovered directly from the Biot–Savart relation with the vorticity, and the vorticity itself is evolved through its transport equation. This is in itself not a new idea (see [22], for example). However, we perform a new analysis of the point vortex approximation to the Biot–Savart integral, and construct explicitly its asymptotic error expansion for rectangular grids. This analysis is used to develop new methods that are efficient and fourth-order accurate.

Traditional numerical methods for fluid mechanics have concentrated on either the primitive variable formulation of velocity-pressure or the vorticity-stream formulation (see [23], for example). A Poisson equation for either the pressure or the stream function is discretized and inverted at each time step with appropriate boundary conditions suitably accounted for. Advantages of these methods include their rapid evaluation and their overall accuracy. They are not so naturally adaptive as an adaptive grid would require inverting an elliptic equation with nonconstant coefficients.

Lagrangian vortex methods (see [10], as well as other references listed at the end of this paper, for example) also exploit the relationship between velocity and vorticity to

*Received by the editors September, 17, 1991; accepted for publication (in revised form) September 30, 1992. The authors were supported in part by National Science Foundation Mathematical Postdoctoral Fellowships.

†Department of Mathematics, Stanford University, Stanford, California 94305. Present address, Department of Mathematics, University of Minnesota, Minneapolis, Minnesota 55455. This work was supported partially by the Office of Naval Research and by the Air Force Office of Scientific Research under grant AFOSR-90-0090.

‡Courant Institute of Mathematical Sciences, New York University, New York, New York 10012.

§Department of Mathematics, University of California, Los Angeles, California 90024.

pose the Euler equations as a closed system of differential equations for the motion of the curvilinear coordinate system moving with the fluid velocity (flow map). Advantages of the Lagrangian methods include their natural adaptivity, ease of implementation, and the existence of fast inversion algorithms [17]. However, their accuracy is difficult to maintain due to grid distortion and the singular nature of the Biot–Savart kernel.

Ideally, one would like to retain the adaptivity of the Lagrangian methods while controlling the grid motion so as to reduce distortion effects and to retain high-order accuracy. An advantage of the vorticity formulation is that adaptive meshes can be incorporated very easily. An adaptive mesh is included by making a specific choice of an underlying coordinate system. This choice of coordinate system merely introduces metric functions in the evolution equation for the vorticity and a Jacobian term in the Biot–Savart integral. In this way, we avoid numerically inverting an elliptic equation with nonconstant coefficients, as we use a discretization of the exact inversion formula. An important side benefit is that there is no ambiguity about the far-field boundary conditions, for open or periodic problems, since they are built into the formula exactly. We view this work as a partial step in the development of such adaptive methods. However, the special case of rectangular grids is very useful and interesting in its own right.

Using an appropriately generalized Poisson summation formula, we construct the full asymptotic error expansion for the point vortex approximation to the Biot–Savart integral evaluated on a rectangular grid. The existence of the error expansion was proved by Goodman, Hou, and Lowengrub [16] more generally on smooth, curvilinear grids, but the method of proof was not constructive. Thus in the case of a rectangular grid, we have provided an explicit example of the expansion. Beginning at the second order, the expansion is in powers of $h^2$, the spatial discretization size. The error is local in that the expansion coefficients depend linearly upon derivatives of the vorticity evaluated only at the mesh point at which the velocity is calculated. In particular, the second-order error term depends only upon the gradient of the vorticity. The error also has a global part in that the coefficients involve two-dimensional lattice sums. However, these sums do not depend on the point of evaluation. These sums are also rapidly convergent except, apparently, at the second order where the sum is only conditionally convergent. We show how this lattice sum can be calculated both easily and rapidly. Thus we can remove the second-order term explicitly from the point vortex approximation to obtain a fourth-order discretization. In the special case of a square grid, even this is unnecessary as the second-order error term is orthogonal to the vorticity gradient. The convective derivative of vorticity is thus calculated to fourth order using the unmodified point vortex approximation, and yields automatically a fourth-order evolution. We also find that in the square grid case, the error expansion contains only powers of $h^4$ after the second-order term. A single Richardson extrapolation to remove the fourth-order term of the point vortex quadrature leaves the second-order and the eighth-order terms remaining. Thus, in the evolution equation, the second-order term falls out to yield eighth-order evolution.

We note that in the case of more general curvilinear grids, extrapolation can be used to generate high-order accurate methods. A difficulty with extrapolation is that although its order of accuracy is higher than the original method, in general, its error coefficients are also larger.

We have also implemented these methods to demonstrate their utility and present numerical results on two difficult test problems. As the point vortex sums over rectangular meshes are discrete convolutions, they are evaluated using the FFT algorithm and the discrete convolution theorem in $O(N^2 \ln N)$ operations where $N^2$ is the number of mesh

points. Vorticity gradients are approximated by high-order difference methods. The first test problem is the nonlinear roll-up of a thin shear layer through the Kelvin–Helmholtz instability. This is a difficult problem as the vorticity develops spatial complexity and steep gradients. The second test problem is the interaction of two oppositely signed vorticies being driven together by an external straining flow. This problem also features strong vorticity gradient production and is relevant to the study of three-dimensional vortex interaction and reconnection [27]. However, the steepest gradients tend to align in a single direction. Consequently, we employ a simple time dependency of the grid to retain resolution of the flow. We compare it to the case where the grid is held fixed. It is a simple, but nontrivial, problem that nicely illustrates how the appropriate choice of time dependency in the grid can greatly improve the calculation.

Our future work includes further consideration of the vorticity transport equation. For example, our time integration method does not make use of the fact that the vorticity equation is a conservation law. The use of methods constructed for such transport equations as essentially nonoscillatory (ENO) methods [19] or other high-order Godunov-type schemes would likely improve the robustness of these methods [7]. It would also be useful to fund the second-order coefficient for the point vortex approximate on a generally smooth, curvilinear coordinate system so that more general fourth-order methods could be constructed without resorting to extrapolation. For the three-dimensional Euler equations, we note that there is a technical difficulty in applying the method developed here to the point vortex approximation. The difficulty involves the sufficiency conditions for applying the special Poisson summation formula for the Biot–Savart kernel (A.29). See Remark 3 at the end of Appendix A. However, we note that the general Poisson summation formula for singular functions (A.9) is still valid. This is currently under study. While the existence of asymptotic error expansions has been proved for the three-dimensional Biot–Savart integral [13], the method is not constructive. Another very important extension is the inclusion of boundaries with and without viscosity. Finally, we note that there is a proof of convergence for a lower-order accurate version of our current method. It will be presented elsewhere.

The outline of the paper is as follows. In §2, we present the method, its implementation, and the special form of its error expansion (the appendices contain the mathematical details of its derivation). In §3, we present some numerical results, and in §4, we give concluding remarks. In Appendix A, the singular Poisson summation formula is derived. In Appendix B, the singular Poisson summation formula is applied to the point vortex discretization of the Biot–Savart integral, and the expansion is proved. In Appendix C, the explicit second-order coefficient is obtained.

**2. The vorticity formulation and smooth grid methods.** The Euler equations for two-dimensional, incompressible fluid flow, in the vorticity formulation, are given by

$$\omega_t + \mathbf{u} \cdot \nabla \omega = 0 \tag{2.1a}$$

and

$$\mathbf{u}(\mathbf{x}, t) = \int_{\mathbf{R}^2} \mathbf{K}(\mathbf{x} - \mathbf{x}')\omega(\mathbf{x}', t)dx_1'dx_2', \tag{2.1b}$$

where $\mathbf{u}(\mathbf{x}, t) = (u_1(\mathbf{x}, t), u_2(\mathbf{x}, t))$ is the fluid velocity, $\omega(\mathbf{x}, t)$ is the scalar vorticity, $\mathbf{x} = (x_1, x_2)$, and

$$\mathbf{K}(\mathbf{x}) = \frac{1}{2\pi|\mathbf{x}|^2}(-x_2, x_1) \tag{2.1c}$$

is the Biot–Savart kernel. Equation (2.1a) expresses that the vorticity in two dimensions is conserved along particle paths, while (2.1b) and (2.1c), the Biot–Savart integral, give the relation between the velocity and the vorticity due to the incompressibility constraint and definition of the vorticity. It is assumed that $\omega$ is smooth and rapidly decaying at infinity.

Although we will soon restrict ourselves to considering the case of rectangular grids, it is instructive to recast the Euler equations in terms of a more general curvilinear coordinate system. Consider the transformation $\mathbf{X}(\mathbf{b},t) = (x_1(b_1,b_2,t), x_2(b_1,b_2,t))$, which, for example, might arise as the solution to the evolution equation

$$\frac{d}{dt}\mathbf{X}(\mathbf{b},t) = \mathbf{F}(\mathbf{X}(\mathbf{b},t),t) \tag{2.2a}$$

for some $\mathbf{F}$. This yields the formulation

$$\frac{d}{dt}\omega(\mathbf{X}(\mathbf{b},t),t) = [(\mathbf{F}(\mathbf{X}(\mathbf{b},t),t) - \mathbf{u}(\mathbf{X}(\mathbf{b},t),t))] \cdot [[\nabla_{\mathbf{b}}\mathbf{X}]^{-1} \cdot \nabla_{\mathbf{b}}\omega] \tag{2.2b}$$

with

$$\mathbf{u}(\mathbf{X}(\mathbf{b},t),t) = \int_{\mathbf{R}^2} \mathbf{K}(\mathbf{X}(\mathbf{b},t) - \mathbf{X}(\mathbf{b}',t))\omega(\mathbf{X}(\mathbf{b}',t),t)J(\mathbf{b}')db_1'db_2', \tag{2.3}$$

where $J$ is the Jacobian of the coordinate transformation given by

$$J = \det\nabla_{\mathbf{b}}\mathbf{X}.$$

A Lagrangian vortex method [10] uses the specific choice $\mathbf{F} = \mathbf{u}$. In this frame, $\mathbf{X}(\mathbf{b},t)$ is the trajectory of a fluid particle along which the vorticity is conserved. Furthermore, the transformation is area preserving due to incompressibility. An Eulerian vortex method, on the other hand, uses the choice $\mathbf{F} = \mathbf{0}$. Here, $\mathbf{X}(\mathbf{b},t) = \mathbf{b}$ and describes a fixed coordinate system. The vorticity is not conserved in this frame and must be advected. The transformation is trivially area preserving.

There are many possible choices of a quadrature method for this integral. For example, there is the point-vortex approximation [22], [26] or quadrature methods based upon mollification of the singular kernel (see [1], [2], [4], [5], [10], [15], [18], [24], for example). We have chosen a fourth-order quadrature method on a rectangular grid that is related to the point vortex method. It has the advantages of ease of implementation, can be summed by a fast method, and is easily generalized to higher orders.

Let the transformation $\mathbf{X}(\mathbf{b},t)$ be discretized uniformly in $\mathbf{b}$. Define $\mathbf{X_j} = \mathbf{X}(\mathbf{b_j},t)$, with $\mathbf{b_j} = (j_1h, j_2h)$. Similar definitions hold for $J$ and $\omega$. Let $\mathbf{I}[\omega]_{\mathbf{j}}$ denote the value of the Biot–Savart integral evaluated at $\mathbf{X_j}$. The point vortex approximation $\mathbf{I}[\omega]_{\mathbf{j}}^0(h)$ is simply the trapezoidal rule approximation to (2.3), where the singular self-induction term is omitted:

$$\mathbf{I}[\omega]_{\mathbf{j}}^0(h) = h^2 \sum_{k\neq j} \mathbf{K}(\mathbf{X_j} - \mathbf{X_k})J_{\mathbf{k}}\omega_{\mathbf{k}}. \tag{2.4}$$

The error is then

$$\mathbf{E}[\omega]_{\mathbf{j}}^0(h) = \mathbf{I}[\omega]_{\mathbf{j}}^0 - \mathbf{I}[\omega]_{\mathbf{j}}^0(h). \tag{2.5}$$

Even though the integrand of the Biot–Savart integral is singular, it was proved by Goodman, Hou, and Lowengrub [16] that there exists a regular asymptotic expansion in powers of $h^2$ for the error. That is, for sufficiently small $h$, there exists constants $\mathbf{C}[\omega]_{\mathbf{j},2p}$ independent of $h$, such that

$$\mathbf{E}[\omega]^0_{\mathbf{j}}(h) = \mathbf{C}[\omega]_{\mathbf{j},2}h^2 + \mathbf{C}[\omega]_{\mathbf{j},4}h^4 + \cdots. \tag{2.6}$$

In general, it appears difficult to find explicit formulae for the coefficients $\mathbf{C}[\omega]_{\mathbf{j},2p}$. For example, in the analysis of Goodman, Hou, and Lowengrub, the second-order coefficient $\mathbf{C}[\omega]_{\mathbf{j},2}$ arises only as an undetermined constant of integration. This particular coefficient is arguably the most useful to know explicitly, as it might then be removed explicitly to yield a higher-order method.

In the special (but very useful) case of a rectangular grid, we give an alternative derivation of the error expansion in which the coefficients $\mathbf{C}[\omega]_{\mathbf{j},2p}$ are given explicitly. We only outline the method here, and refer the interested reader to the appendices for the full details. The main tool is the Poisson summation formula generalized to singular functions. The Poisson summation formula (see, for example, [14]) expresses the trapezoidal sum (say, over the plane) as a sum of Fourier coefficients of the summand. The asymptotic behavior of these Fourier coefficients then allows an analysis of the error in the trapezoidal approximation. However, the integrand of (2.1b) lacks the smoothness necessary for direct application of the Poisson summation formula, which, if used naively, leads to sums of Fourier coefficients that are not absolutely, but only conditionally, convergent. The value of such a sum depends upon how the sum is evaluated. Instead, the integrand of (2.1b) is first smoothed by convolution with an approximate $\delta$-function $\delta_\epsilon$ of width $\epsilon$. The Poisson summation formula is then applied to the trapezoidal approximation of the smoothed integral and the limit $\epsilon \to 0$ is taken. This leads to the Poisson summation formula generalized to singular functions. The particular choice of $\delta_\epsilon$ leads to a particular interpretation of the conditionally convergent sum, and produces a compensating residue from the singular self-induction term omitted in (2.4). We have chosen $\delta_\epsilon$ so as to actually yield rapidly and absolutely convergent sums, and an explicitly calculable residue term.

There is at least an apparent difficulty in applying these methods to the general curvilinear case to find *explicit* expressions for the error coefficients. We would require the Fourier transform of the kernel $\mathbf{K}(\mathbf{X}(\mathbf{b}))$ in the $\mathbf{b}$ variable. This is not generally known.

Let $\mathbf{X}_\mathbf{j} = (j_1h_1, j_2h_2) = (j_1\alpha_1 h, j_2\alpha_2 h)$ be the rectangular grid. Let $\omega_{x_2,\mathbf{j}}$ denote the value of $\omega_{x_2}$ evaluated at $\mathbf{X}_\mathbf{j}$, and similarly for $\omega_{x_1,\mathbf{j}}$. The point vortex approximation is now simply

$$\mathbf{I}[\omega]^0_{\mathbf{j}}(h) = h_1h_2 \sum_{\mathbf{k}\neq\mathbf{j}} \mathbf{K}((j_1-k_1)h_1, (j_2-k_2)h_2)\omega_{\mathbf{k}}. \tag{2.7}$$

We then have the following theorem.

ERROR EXPANSION THEOREM. *Let $\omega(\mathbf{x})$ be smooth and rapidly decaying and $\alpha = \alpha_1/\alpha_2$.*

*Part* A. *The second-order error coefficient is given by*

$$\mathbf{C}[\omega]_{\mathbf{j},2}h^2 = \left(\frac{-\omega_{x_2,\mathbf{j}}}{4\pi}C_2(\alpha), \frac{\omega_{x_1,\mathbf{j}}}{4\pi}C_2(1/\alpha)\right) h_1h_2, \tag{2.8a}$$

*where*

$$C_2(\alpha) = \frac{4}{\pi}\arctan(1/\alpha) - \frac{4\alpha}{\pi}\sum_{m=1}^{\infty}\frac{1}{m}f(m;\alpha), \tag{2.8b}$$

*and*

$$f(m;\alpha) = \frac{1}{m}{\sum_{l=0}^{m}}'\left(\frac{(l/m)^2-\alpha^2}{((l/m)^2+\alpha^2)^2} + \frac{1-\alpha^2(l/m)^2}{(1+\alpha^2(l/m)^2)^2}\right). \tag{2.8c}$$

*By $\sum'$ is meant the trapezoidal sum; that is, the terms at $l = 0$ and $m$ are weighted by a factor of $\frac{1}{2}$.*

*Remark* 1. In the special case of a square grid ($\alpha = 1$), $C_2(\alpha) = C_2(1/\alpha) = 1$, and it follows that

$$\mathbf{C}[\omega]_{\mathbf{j},2} = \frac{1}{4\pi}\nabla^{\perp}\omega|_{\mathbf{j}h}, \tag{2.9}$$

where $\nabla^{\perp}\omega = (-\partial_{x_2}, \partial_{x_1})\omega$ is the perpendicular gradient of $\omega$. Thus, the second-order error term in (2.4) is orthogonal to $\nabla\omega$ (i.e., $h^2\nabla^{\perp}\omega\cdot\nabla\omega = 0$), and the method of lines discretization of (2.1a), is

$$\frac{d}{dt}\omega_{\mathbf{j}}^h = -\mathbf{I}[\omega^h]_{\mathbf{j}}^0(h)\cdot(\nabla_h\omega^h)_{\mathbf{j}}, \tag{2.10}$$

where $\nabla_h$ is an approximation to $\nabla$ to at least fourth order. Equation (2.10) then has a fourth-order consistency error in space, even though the velocity approximation is only second order. That this error is realized in numerical simulations of fluid motions will be demonstrated in the next section.

*Remark* 2. For the case of the rectangular grid, the calculation of the coefficient $C_2(\alpha)$ appears formidable. And indeed, a straightforward implementation of the sum (2.8b), for $\alpha = 2$, produces summands of the size $10^{-14}$ only by $m = 12600$. Fortunately, the convergence of this sum can be considerably improved by using the Euler–MacLaurin summation formula (see, for example, [29]) to successively remove the dominant behavior of the summand. From the summation formula applied to (2.8c), we have for $m >> 1$,

$$\begin{aligned} f(m;\alpha) &= \frac{1}{6}\frac{\alpha^2-1}{(1+\alpha^2)^2}\frac{1}{m^2} - \frac{1}{30}\frac{(\alpha^2-1)(\alpha^4-10\alpha^2+1)}{(1+\alpha^2)^4}\frac{1}{m^4} + O\left(\frac{1}{m^6}\right) \\ &= f_2(\alpha)\frac{1}{m^2} + f_4(\alpha)\frac{1}{m^4} + O\left(\frac{1}{m^6}\right). \end{aligned}$$

Thus, we can rewrite the sum in (2.8b) as

$$\begin{aligned} \sum_{m=1}^{\infty}\frac{1}{m}f(m;\alpha) = \sum_{m=1}^{\infty}\frac{1}{m}\left[f(m;\alpha) - f_2(\alpha)\frac{1}{m^2} - f_4(\alpha)\frac{1}{m^4}\right] \\ + f_2(\alpha)\zeta(3) + f_4(\alpha)\zeta(5), \end{aligned} \tag{2.11}$$

where

$$\zeta(s) = \sum_{m=1}^{\infty}\frac{1}{m^s}, s > 1,$$

is the Riemann zeta function. In particular, $\zeta(3) = 1.202056903159594$ and $\zeta(5) = 1.036927755143370$. The sum in (2.8b) now converges as $O((1/m)^7)$, and is trivial to compute; for $\alpha = 2$, the above formula produces summands of magnitude $10^{-14}$ by $m = 45$. Figure 1 shows $C_2(\alpha)$ calculated by the above formulae.

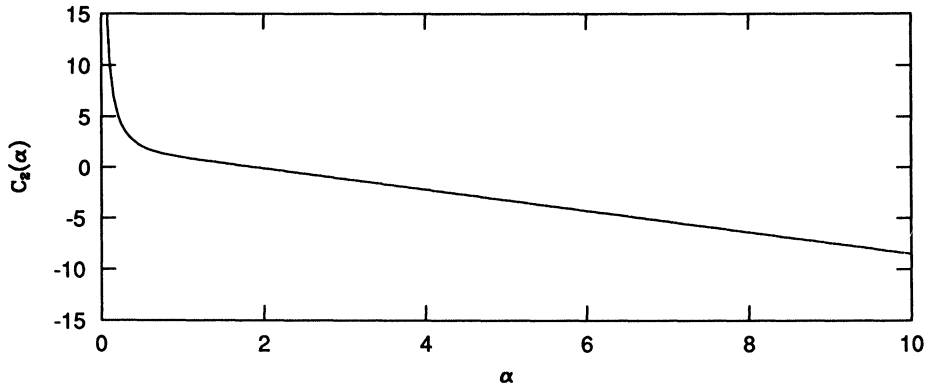



FIG. 1. *The second-order error coefficient* $C_2(\alpha)$.

*Remark* 3. We can use the calculation of $C_2(\alpha)$ to obtain a fourth-order quadrature rule for the Biot–Savart integral by subtracting the second-order term

$$\tilde{\mathbf{I}}_{\mathbf{j}}(h) = \mathbf{I}[\omega]^0_{\mathbf{j}}(h) - \left( \frac{-\omega^h_{x_2,\mathbf{j}}}{4\pi} C_2(\alpha), \frac{\omega^h_{x_1,\mathbf{j}}}{4\pi} C_2(1/\alpha) \right) h_1 h_2. \tag{2.12}$$

We have assumed that $\omega_{x_2,\mathbf{j}}$ and $\omega_{x_1,\mathbf{j}}$ are approximated to at least fourth order by $\omega^h_{x_2,\mathbf{j}}$ $\omega^h_{x_1,\mathbf{j}}$. Use of this formula requires little effort, since for the calculation of $\omega_t$, these spatial derivatives must be approximated anyway.

*Remark* 4. That the error coefficients only depend on derivatives of $\omega$ at $\mathbf{X}_{\mathbf{j}}$ is true also for the higher-order coefficients. This type of expression for $\mathbf{C}[\omega]_{\mathbf{j},2}$ is also very similar to that derived by Sidi and Israeli [29] for quadrature rules of one-dimensional integrals with Cauchy singularities, and which was subsequently used by Shelley [28] in a study of singularity formation in vortex sheet motion.

*Remark* 5. The second-order error coefficient (2.8a) can also be found without recourse to the Poisson summation formula. This is done by dividing the quadrature error (2.5) into local and nonlocal contributions. The nonlocal contributions can be estimated by using the Euler–MacLaurin summation formula, and the local contributions lead to sums similar to those in (2.8). It may be that the more general curvilinear case could be handled by such an approach. Furthermore, in the case of the square grid, the expression of $\mathbf{C}[\omega]_{\mathbf{j},2}$, (2.9), can be found by manipulating both integral and sum so as to have a smoother integrand and summand, to which standard quadrature estimates can then be applied.

*Part* B (*Error Expansion Theorem*). *The higher-order error coefficients* ($p > 1$) *are given by*

$$\mathbf{C}[\omega]_{\mathbf{j},2p} = \frac{1}{(2\pi)^{2p}} \sum_{\substack{r,q \\ r+q=2p-1}} (-D^{q,r}(\alpha)[\omega], D^{r,q}(1/\alpha)[\omega])|\mathbf{x}_{\mathbf{j}}, \tag{2.13}$$

*where $D^{r,q}(\alpha)$ is a linear differential operator of order $r$ in $x_1$ and order $q$ in $x_2$, and whose coefficients depend upon $\alpha, r$, and $q$.*

*Remark* 6. The operator $D^{q,r}(\alpha)$ involves lattice sums analogous to those in (2.8). These sums are absolutely convergent, and their values are independent of the choice of smoothing function $\delta_\epsilon$. It is only the second-order coefficient for which there is a question of interpretation of the sum.

*Remark* 7. In the special case of a square grid ($\alpha = 1$), it can be shown that $\mathbf{C}[\omega]|_{\mathbf{j},2p} = \mathbf{0}$ for $p > 1$ and odd. That is, after the $h^2$ term, the expansion has only powers of $h^4$. Thus, an eighth-order method could be easily obtained by performing one Richardson extrapolation of the point vortex approximation to remove the fourth-order term. The second-order and eighth-order terms remain, but the second-order term disappears in the evolution equation as before.

The proof of the error expansion theorem is given in the appendices. In Appendix A the derivation of the Poisson summation formula for singular functions is given. In Appendix B, the extended Poisson summation formula is used to rigorously derive the coefficients $\mathbf{C}[\omega]_{\mathbf{j},2p}$ of the error expansion (2.6). In Appendix C, the second-order error term is expressed in terms of rapidly convergent series as given in (2.8).

It has now been shown how, for rectangular grids, fourth-order methods can be found by a trivial and explicit removal of the second-order error (and even this was not necessary in the square grid case). We also note that the point vortex approximation can be evaluated very efficiently in this case. Equation (2.7) can be written as

$$\mathbf{I}[w]_{\mathbf{j}}^0 h = \sum_{\mathbf{k}} \tilde{\mathbf{K}}_{\mathbf{j}-\mathbf{k}} \omega_{\mathbf{k}}, \tag{2.14}$$

where

$$\tilde{\mathbf{K}}_{\mathbf{j}} = h_1 h_2 \mathbf{K}(j_1 h_1, j_2 h_2).$$

That is, (2.14) is a discrete convolution. In such cases, through the discrete Fourier transform and its associated discrete convolution theorem, the FFT algorithm can be used to evaluate such sums very rapidly. To employ these techniques, the kernel $\tilde{\mathbf{K}}_{\mathbf{j}}$ and vorticity $\omega_{\mathbf{j}}$ must be extended appropriately as periodic functions, and then represented as discrete Fourier transforms. The details of this are straightforward and will not be given here. For a rectangular mesh the computational complexity of forming the velocity on the mesh is thus $O(N^2 \ln N)$, where $N$ is the number of grid points in each direction. There are now very well developed multidimensional FFT packages that are highly vectorized, and that realize the asymptotic complexity of the algorithm for relatively small values of $N$.

In the more general case of a curvilinear coordinate system, the existence of the error expansion also allows the derivation of higher-order methods through Richardson extrapolation. Here we give explicitly a fourth-order formula. Using

$$\mathbf{E}[\omega]_{\mathbf{j}}^0(2h) = \mathbf{I}[\omega]_{\mathbf{j}} - \mathbf{I}[\omega]_{\mathbf{j}}^{2h} = 4\mathbf{C}[\omega]_{\mathbf{j},2} h^2 + 16\mathbf{C}[\omega]_{\mathbf{j},4} h^4 + \cdots$$

together with (2.5), we find that defining the new quadrature rule $\mathbf{I}[\omega]_{\mathbf{j}}^1(h)$ by

$$\mathbf{I}[\omega]_{\mathbf{j}}^1(h) = \frac{1}{3}\left[4\mathbf{I}[\omega]_{\mathbf{j}}^0(h) - \mathbf{I}[\omega]_{\mathbf{j}}^0(2h)\right] = \frac{4}{3}h^2 \sum_{\substack{j_1+k_1 \text{ odd} \\ \text{or} \\ j_2+k_2 \text{ odd}}} \mathbf{K}(\mathbf{X}_{\mathbf{j}} - \mathbf{X}_{\mathbf{k}}) J_{\mathbf{k}} \omega_{\mathbf{k}} \tag{2.15}$$

and gives the error

$$\mathbf{E}[\omega]_{\mathbf{j}}^{1}(h) = \mathbf{I}[\omega]_{\mathbf{j}} - \mathbf{I}[\omega]_{\mathbf{j}}^{1}(h) = -12\mathbf{C}[\omega]_{\mathbf{j},4}h^4 + \cdots. \tag{2.16}$$

A method of lines treatment of (2.2b) would then have the form

$$\frac{d}{dt}\omega_{\mathbf{j}}(t) = [(\mathbf{F}(\mathbf{X}_{\mathbf{j}}(t), t) - \mathbf{I}[\omega(t)]_{\mathbf{j}}^{1}(h))] \cdot [\nabla_{h,\mathbf{b}}\mathbf{X}]_{\mathbf{j}}^{-1} \cdot (\nabla_{h,\mathbf{b}}\omega)_{\mathbf{j}}. \tag{2.17}$$

Obviously, further extrapolations to gain higher order could be done computationally, or by calculation of the specific formula. However, we note that further extrapolations would involve computing further doublings of the mesh size, which generally leads to larger error coefficients in the error expansions.

The fourth-order quadrature method given by (2.15), $\mathbf{I}[\omega]_{\mathbf{j}}^{1}(h)$, can be efficiently implemented in a number of ways. If the grid is nonrectangular, then fast summation techniques such as those using hierarchical elements [1], or multipole expansions [17] can be employed. Equation (2.15) can be interpreted as dividing the grid into four interlaced subgrids, as shown in the schematic in Fig. 2. Each grid point is labeled as belonging to subgrid $M_1$, $M_2$, $M_3$, or $M_4$. Then the quadrature rule $\mathbf{I}[\omega]_{\mathbf{j}}^{1}(h)$ for $\mathbf{b}_{\mathbf{j}} \in M_i$ becomes

$$\mathbf{I}[\omega]_{\mathbf{j}}^{1}(h) = \frac{4}{3}h^2 \sum_{\mathbf{b}_{\mathbf{k}} \notin M_i} \mathbf{K}(\mathbf{X}_{\mathbf{j}} - \mathbf{X}_{\mathbf{k}}) J_{\mathbf{k}}\omega_{\mathbf{k}}. \tag{2.18}$$

Thus, this fourth-order quadrature rule for the Biot–Savart integral is seen as an abstracted point vortex approximation, where instead of a singular self-interaction term being omitted, a subgrid of quadrature points is omitted. Also, the set of field points $M_1$ all use the same set of vortex points $M_2$, $M_3$, and $M_4$ to find the velocity on $M_1$, and the quadrature weights are independent of the field point position. These are the types of quadrature rules to which fast summation methods are applicable. In principle, fast summation methods based on multipole expansions or hierarchical elements have computational complexities of $O(N^2)$ or $O(N^2 \ln N)$. However, we have not found these methods to be competitive in evaluating the sum when summation using the FFT can be employed.

**3. Some numerical results.** We have implemented these methods to numerically solve two incompressible open-flow problems of enduring interest. The first is the nonlinear roll-up of a thin shear layer through the Kelvin–Helmholtz instability. The second is the interaction of two oppositely signed vortices being driven together by an external straining flow.

For a flow periodic in one direction (say, $2\pi$-periodic in $x_1$), the Biot–Savart integral can be summed exactly over each period to yield an integral, with modified kernel, over a single periodic strip. In particular, $\mathbf{K}$ in (2.1c) is replaced by

$$\mathbf{K}_{\text{per}}(x_1, x_2) = \frac{1}{4\pi} \frac{(-\sinh(x_2), \sin(x_1))}{\cosh(x_2) - \cos(x_1)},$$

and the domain of integration is $[0, 2\pi] \times (-\infty, +\infty)$. We assume that the vorticity is rapidly decaying as $|x_2| \to \infty$.

We consider the initial data

$$\omega(x_1, x_2) = -\exp(-\alpha(x_1)^2 x_2^2),$$

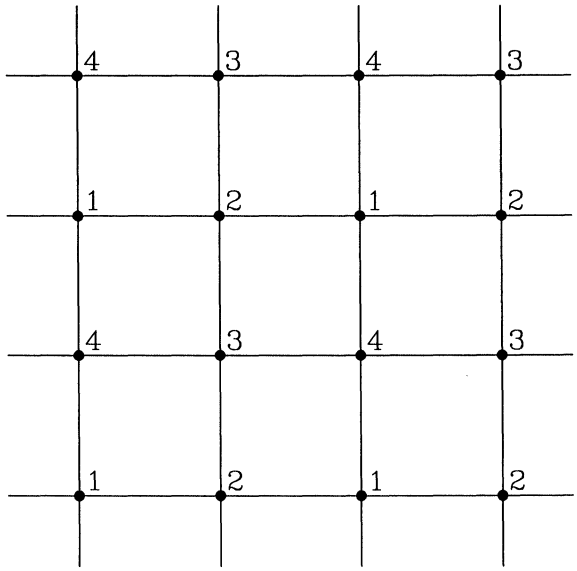



FIG. 2. *A schematic of the four-grid decomposition, $M_1$, $M_2$, $M_3$, and $M_4$.*

where $\alpha(x_1)^2 = \beta[1+\epsilon(\cos x_1 - 1)]$. That is, $\omega$ describes a flat shear layer of characteristic width $1/\sqrt{\beta}$, whose width is sinusoidally perturbed with nondimensional amplitude $\epsilon$. If the vorticity amplitude were likewise scaled as $\sqrt{\beta}$ (fixing the circulation independently of $\beta$) and $\beta \to \infty$, this would yield vortex sheet initial data with an initially flat sheet and a sinusoidal perturbation to a constant vortex sheet strength.

We have chosen $\beta = 10$ and $\epsilon = .1$. This is a fairly thin shear layer with aspect ratio of about 20:1. As this flow develops very steep gradients in the vorticity, it is a severe test of any method. Figures 3(a)–3(d) show contours of the evolving vorticity at the times $t = 0$, 20, 25, and 30, respectively. The computational domain is $[0, 2\pi] \times [-5\pi/8, 5\pi/8]$ and vorticity is initially of the size $2 \cdot 10^{-17}$ on the upper and lower boundaries. Figures 3(a)–3(c) are with $N_1 = 512$ and $N_2 = 320$, and Fig. 3(d) is with $N_1 = 1024$ and $N_2 = 640$. The tick marks on the box boundaries correspond to the grid. These choices for $N_1$ and $N_2$ give a square mesh covering the computational domain. The contour lines are from $-0.95$ up to $-0.05$ at intervals of 0.05.

Here, the velocity on the grid is computed by the point vortex approximation (2.7) using the periodic kernel $\mathbf{K}_{\text{per}}$, and the sums are evaluated rapidly using the FFT. By scaling both $N_1$ and $N_2$ as $N$, the amount of work per time step is then $O(N^2 \ln N)$. On a Cray Y-MP, with $N_1 = 1024$ and $N_2 = 640$, evaluation of the velocity took about one second. The vorticity gradient is computed by cubic splines in each direction, assuming periodic boundary conditions in the $x_1$-direction, and zero data on the upper and lower boundaries. Cubic splines with such boundary conditions yield fourth-order derivative approximations on the mesh points. Then, since $h_1 = h_2$, and by Remark 1 of §2, the method of lines discretization (2.10) of the vorticity transport equation (2.1a) has a fourth-order spatial consistency error. The method of time integration used is a fourth-order, Adams–Moulton predictor-corrector method. The time step was $\Delta t = .00625$, which, for the $N_1 = 1024$ calculation, was halved at $t = 20$ to satisfy the CFL condition.

The time steps used are small enough to effectively remove time discretization errors from the calculation.

Figures 3(a)–3(d) trace the usual course of vortex layer roll-up (see, for example, [3] for such calculations with layers of constant vorticity). The Kelvin–Helmholtz instability initially causes vorticity to advect towards the center, leading to a relative concentration there (see Fig. 3(b)). The layer rolls up subsequently and forms a central rotating vortex with trailing arms. As the vorticity is strained into the center, the outer arms thin and large gradients in the vorticity are created there. As the contour lines are also material curves for the flow, their considerable stretching and folding likewise lead to large gradients.

The error in the calculations can be estimated through use of its asymptotic expansion. For example, by assuming that for the vorticity

$$E^h_{\omega,\mathbf{j}} = \omega_{\mathbf{j}} - \omega^h_{\mathbf{j}} = A_4 h^4 + A_6 h^6 + \cdots, \tag{3.1}$$

we then have the estimate

$$E^h_{\omega,\mathbf{j}} = \frac{\omega^{2h}_{\mathbf{j}} - \omega^h_{2\mathbf{j}}}{2^4 - 1} + O(h^6). \tag{3.2}$$

Then

$$L_{h,\infty}[\omega] = \max_{\mathbf{j}} \left| \frac{\omega^{2h}_{\mathbf{j}} - \omega^h_{2\mathbf{j}}}{2^4 - 1} \right| \tag{3.3}$$

is an approximation to maximum error in the vorticity.

The left-hand box in Fig. 4 shows $L_{h,\infty}[\omega]$ (solid) and $L_{h,\infty}[u]$ (dashed) for $h = 2\pi/N_1$ with $N_1 = 128, 256, 512$, and 1024 for $0 \le t \le 30$, while the right-hand box shows the order of the calculations approximated by the expression $\log_2(L_{2h,\infty}/L_{h,\infty})$. Here $u$ is the velocity in the $x_1$-direction and is calculated on the grid using (2.12). All the evidence suggests a stable and convergent scheme. For a single calculation, the error shows a monotonic increase as the layer rolls up. This is hardly surprising (referring to Figs. 3(a)–3(d)); gradients of vorticity evolving under the Euler equations grow very rapidly, and in fact obey an evolution equation similar to that for the vorticity vector in three dimensions. As the resolution is improved, the accuracy is improved upon the entire range of integration. The approximation of the order shows a clear fourth-order error for a range of time that increases as the resolution is improved. The velocity error shows generally a slower decrease than does the vorticity error. This is true as well for the decrease away from fourth-order error. This is likely a consequence of the velocity being one degree smoother than the vorticity.

A difficulty of the $L_{h,\infty}$ measure of the error in $\omega^h$ is that it assumes that $\omega^{2h}$ is still well represented by (3.1). Other measures of the error, which do not depend as strongly on expansion (3.1), are the approximated circulation and maximum vorticity. For this flow the circulation $C$ in a periodic strip is a conserved quantity. The graph at the left in Fig. 5 shows $-\log_{10}|C - C_h|$, as a function of time, for the four successive doublings of the mesh size beyond $N_1 = 64$. $C_h$ is calculated using the trapezoidal rule over the computational box, which would be of infinite order in the absence of discretization errors in $\omega$ (this explains the very high accuracy at $t = 0$). The calculated order of the convergence is shown in the graph at right, and the fourth-order convergence is seen clearly over nearly the entire range of integration. We note however that the circulation is an integral measure of the error, and as such is a weak measure of accuracy.

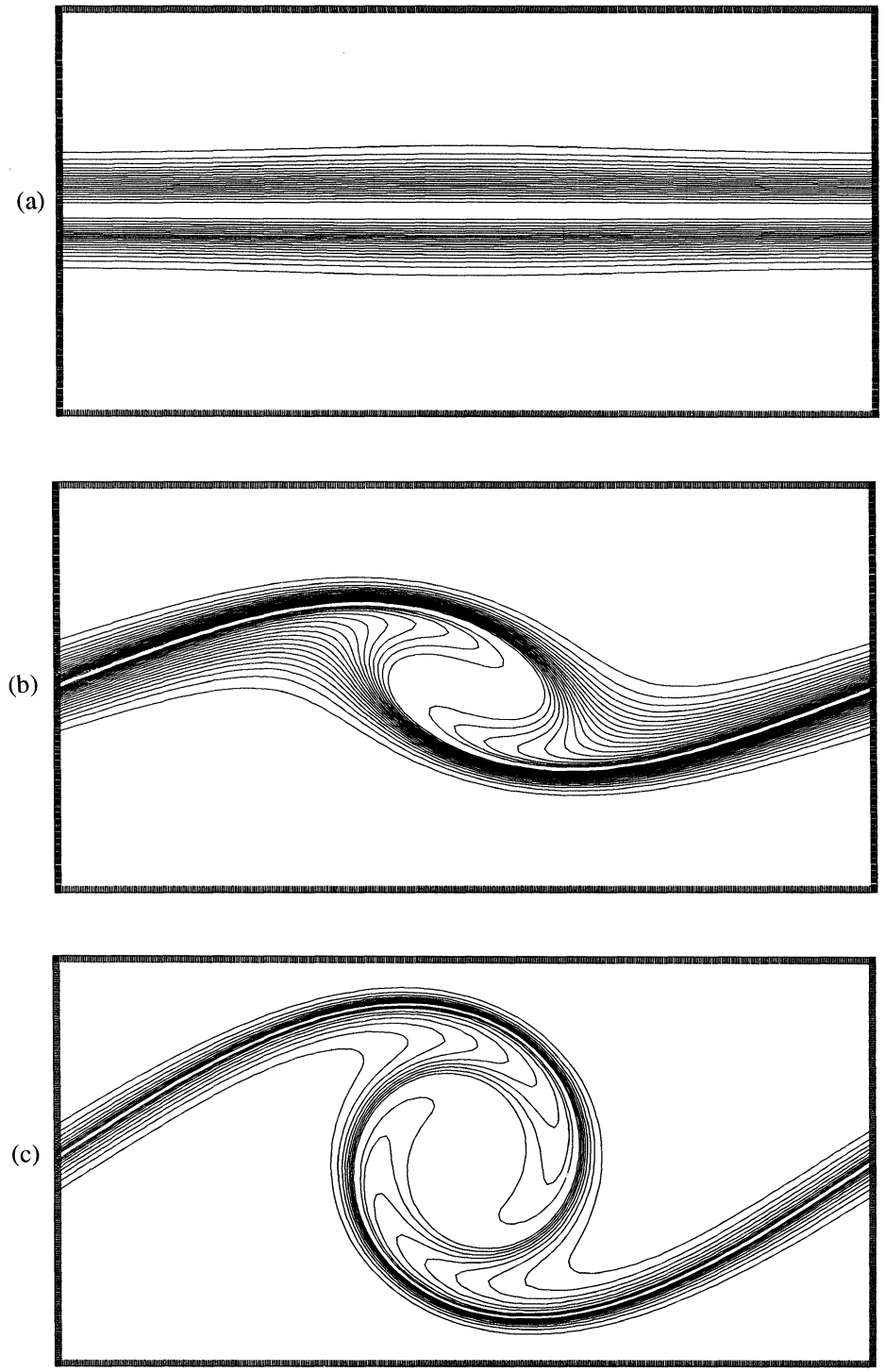



FIG. 3. *Contours of the vorticity for an evolving thin shear layer at times* $t = 0, 20, 25,$ *and* 30. *The contour levels run from* $-0.95$ *to* $-.05$, *at intervals of* .05.

(d)

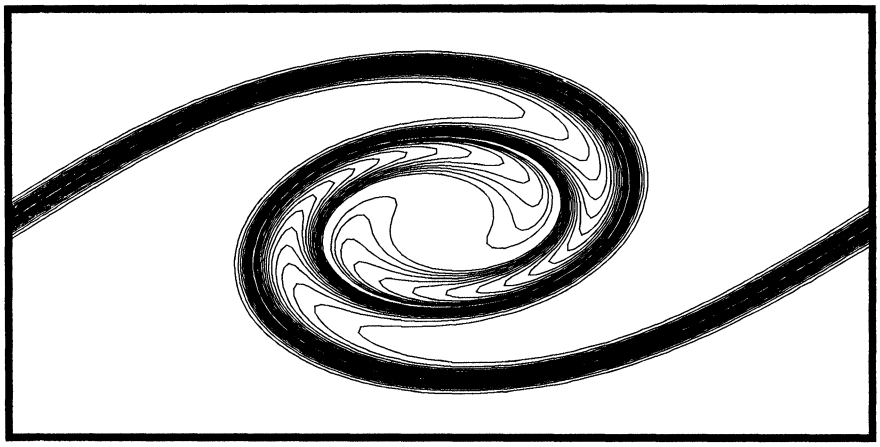


FIG. 3. *Continued.*

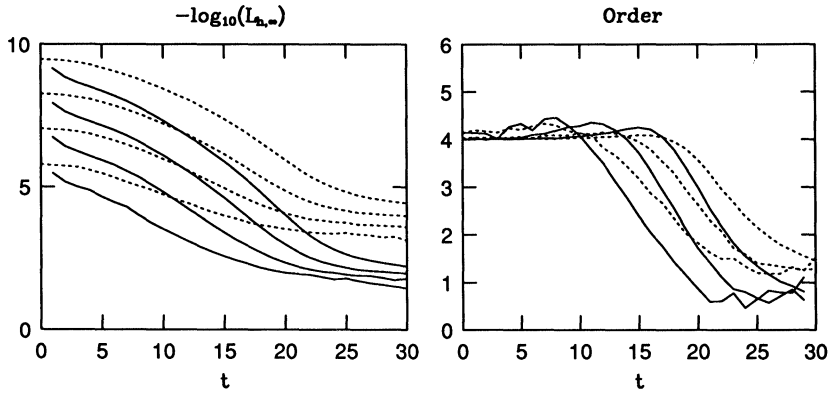



FIG. 4. *The approximated error in vorticity (solid) and velocity (dashed) for* $h = 2\pi/N_x$ *with* $N_x = 128, 256, 512,$ *and* $1024$ *for* $0 \leq t \leq 30$. *The accuracy improves as N is increased. The right-hand box shows the order of the calculations.*

Another invariant of the two-dimensional Euler equations is $\|\omega\|_\infty$, the maximum modulus of the vorticity. This quantity must be estimated point-wise. As such, it is a stronger measure of error than the circulation. Figure 6 shows $\|\omega\|_{h,\infty}$, or the maximum vorticity on the mesh, for the five different resolutions. For the initial condition used, $\|\omega\|_\infty = 1$, and $|\omega(x_1, x_2, t = 0)| = 1$ along the entire curve $x_2 = 0$. While convergence is plainly seen, the spatial location of the maximum value jumps around the mesh as the flow evolves, and it is difficult to estimate an order of convergence from this quantity. We note specifically, that for the calculation with $N_1 = 1024$ and $N_2 = 640$, $\|\omega\|_{h,\infty} \simeq 1.001$ at $t = 30$.

We have also performed these calculations using the more general fourth-order point vortex approximation (2.15), obtained by extrapolation of the second-order quadrature. The extrapolated method also shows fourth-order convergence, and appears stable

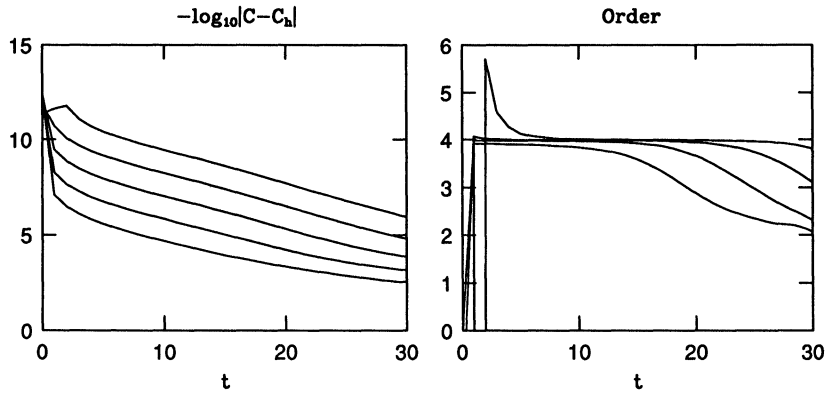



FIG. 5. *The error in circulation, with its approximation calculated by using the trapezoidal rule over the computational box for* $N_x = 64, 128, 256, 512,$ *and* 1024. *The accuracy improves as N is increased. The right-hand box shows the orders of the computations.*

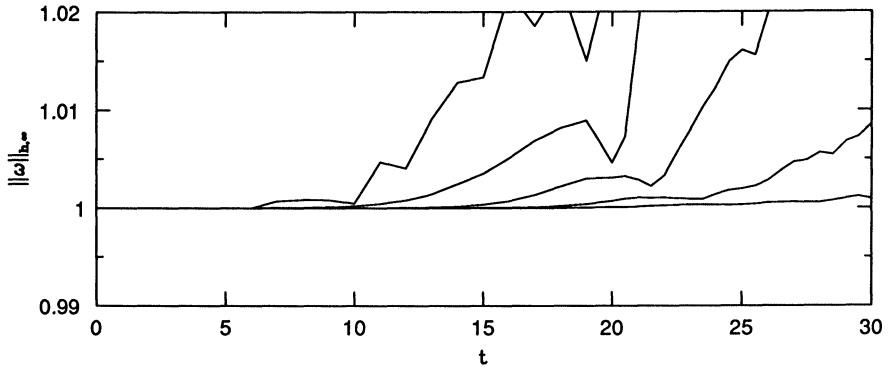



FIG. 6. *The maximum vorticity on the grid* $\|\omega\|_{h,\infty}$ *for* $N_2 = 64, 128, 256, 512,$ *and* 1024. *The difference from* 1 *decreases as N is increased.*

and convergent. Its associated errors are typically larger by about a factor of twelve than those associated with using (2.10), which is consistent with the change in the fourth-order error coefficient introduced by the extrapolation.

We now consider a much different problem. We calculate the motion of two oppositely signed vortices that interact under the imposition of an external straining flow. This problem features a strong vorticity gradient production that quickly taxes any method. However, the steepest gradients tend to be aligned in a single direction, and the introduction of a simple time-dependency of the grid helps retain resolution of the flow. The behavior of such flows is relevant to the study of three-dimensional vortex interaction and reconnection (see, for example, [27]). It is a simple, but nontrivial, problem that nicely illustrates how appropriate choice of time dependency in the grid motion can greatly improve the accuracy of a calculation.

Consider special solutions to the three-dimensional Euler equations that are of the form

$$\begin{aligned}\mathbf{U} &= (u, v, w)\\ &= (\tilde{u}(x_1, x_2, t) - \gamma x_1, \tilde{v}(x_1, x_2, t) + \beta x_2, \tilde{\omega}(x_1, x_2, t) + (\gamma - \beta)x_3).\end{aligned} \tag{3.4}$$

Here, while there are components of velocity and vorticity in all three directions, the only true $x_3$-dependency is through the irrotational and incompressible straining field

$$(-\gamma x_1, \beta x_2, (\gamma - \beta)x_3).$$

For solutions of this form, the full Euler equations reduce to two-dimensional evolution equations for $u$ and $v$, in which the only effect of the velocity component $w$ is through the rate-of-strain in that direction, namely, $\gamma - \beta$. Here, $w$ is simply advected as a scalar field in the two-dimensional velocity field $\mathbf{V} = (\tilde{u} - \gamma x_1, \tilde{v} + \beta x_2)$. In terms of the scalar vorticity $\omega = v_{x_1} - u_{x_2} = \tilde{v}_{x_1} - \tilde{u}_{x_2}$, the evolution equations can be given in a form very similar to equation set (2.1). Namely,

$$\omega_t + \mathbf{V} \cdot \nabla\omega = \omega(\gamma - \beta), \tag{3.5a}$$

and

$$(\tilde{u}, \tilde{v})(\mathbf{x}, t) = \int_{\mathbf{R}^2} \mathbf{K}(\mathbf{x} - \mathbf{x}')\omega(\mathbf{x}', t)dx_1' \, dx_2', \tag{3.5b}$$

where $\mathbf{K}$ is defined as before by (2.1c). As initial data we take

$$\omega(\mathbf{x}, 0) = a(\exp((x_1 - 1/2)^2 + x_2^2)/d^2 - \exp((x_1 + 1/2)^2 + x_2^2)/d^2). \tag{3.6}$$

The initial vorticity is then two Gaussian cores of opposite sign and with width $d$, centered at $\pm 1/2$. The rates-of-strain are set as $\gamma = 2$ and $\beta = 1$. That is, there is a compressive external flow in the $x_1$-direction that pushes the two vortices together and extensional flows in the $x_2$ and $x_3$-directions. The extensional rate-of-strain in the $x_2$-direction elongates the vortices in that direction, while that in $x_3$ leads to vortex stretching. Furthermore, we choose $a = 10$ and $d = 1/4$.

Such a flow could be considered as a model for the interaction of two adjacent vortices being driven together by strains induced by other vorticity distributions in the flow, or as a model of the effect of three-dimensional vortex tube curvature, where the two vortices are cross sections of two adjacent vortex tubes. Such a flow illustrates the effect of external strains producing core deformation and thus altering the interaction of the vortices with each other.

The primary difficulty in computing such a flow is that as the two vortices are driven together by the external straining flow, large gradients are rapidly produced in the vorticity. To maintain good resolution of the flow, we found it necessary to introduce a simple time dependence of the grid. Namely, we allowed the grid to collapse with the compressive strain in the $x_1$-direction, so as to maintain resolution of the sharp vertical gradients that have formed. In addition, as two vortices translate vertically through their mutually induced velocities, the $x_2$-position of the grid must be chosen accordingly so that the vorticities are kept within the computational domain. That is,

$$\frac{d}{dt}x_1(\mathbf{b}, t) = -\gamma x_1(\mathbf{b}, t) \quad \text{with } x_1(\mathbf{b}, t = 0) = b_1,$$

$$\frac{d}{dt}x_2(\mathbf{b}, t) = \bar{v}_2(t) \quad \text{with } x_2(\mathbf{b}, t = 0) = b_2,$$

where $\bar{v}_2(t)$ is chosen to keep the $x_2$-centroid of the vortices fixed at $x_2 = 0$. This requires the computation of the circulation, the $x_2$-centroid and its time derivative all on a half-plane of the domain (since the circulation over the whole domain is zero). We calculated these integrals on the right half-plane by Simpson's rule. This choice maintains a rectangular grid.

For this time-dependent coordinate system we can find $\nabla_{\mathbf{b}}\mathbf{X}$ in closed form, and thus also the Jacobian $J$ for (2.3). Thus, we can evolve the vorticity transport equation (2.2b) (with the forcing term from the strain included). More importantly, the grid is no longer square, and the point vortex approximation (2.7) does not yield a fourth-order evolution without modification. Accordingly, we now use the quadrature rule (2.12), where $C_2(\alpha(t)), \alpha = h_1/h_2$, must be calculated at each time step. As noted in Remark 2 of §2, this can be done easily and rapidly through the use of formula (2.11), and only requires $\nabla\omega$, whose computation is already necessary. Again, it is assumed that $\omega$ is zero on the boundaries. For variety we use fourth-order differences rather than splines to calculate $\nabla\omega$. This appears to have little effect on the computation.

Figures 7(a)–7(c) show the contours of the computed vorticity field at $t = 0, .5$ and 1.0 with $N_1 = N_2 = 256$ and $\Delta t = .00078125$. The perimeter in Figs. 7(a)–7(c) is the boundary of the time-dependent computational domain. The computational box is initially of length 4.2 on a side. The time step was chosen small enough to effectively remove time discretization errors from this calculation (as well as the calculation where the initial $x_1$-positions of the grid were held fixed).

Figure 8 shows the errors in $\omega$ (solid) and $u$ (dashed), as well as their orders, as approximated by (3.3). The errors in $\omega$ are normalized by the maximum vorticity, $\|\omega\|_\infty(t) = a\exp(\gamma - \beta)t$. Here, $N_1 = N_2 = 128$ and 256. This is to be contrasted with Fig. 9, which shows the same quantities, but for the same calculations with the initial $x_1$-grid locations held fixed. The errors for the calculation with the moving grid is much smoother in time, and increase more slowly. Indeed, by $t = 0.4$, the moving grid calculation with $N_1 = 128$ is as accurate as that for the fixed grid with $N_1 = 256$, and becomes more accurate (by virtue of its slower increase) by the end of the calculation.

The total conserved circulation of the two vortices is zero. However, it is also true that circulation computed from vorticity of a single sign is conserved, and in particular the circulation in the left or right half-plane is conserved (note that $x_1 = 0$ is a free-slip surface for this flow). Figure 10 shows the error in the circulation for the right-hand vortex (calculated on the right half-plane using Simpson's rule), and its computed order, for the moving (solid) grid calculation at the three resolutions $N_1 = N_2 = 64, 128$, and 256 and the fixed (dashed) grid at the $N_1 = N_2 = 256$ resolution. This figure only serves to further illustrate the advantage in accuracy the moving grid affords over the fixed calculation. There is a slight degradation in accuracy near $t = 1$ for the $N_1 = N_2 = 256$ calculation. This is due to the vertical boundary (upon which the vorticity and its derivatives are assumed to be zero) coming too close to the support of the vorticity. The lower resolution runs are less sensitive to such a boundary effect. Figure 11 shows the normalized maximum vorticity on the mesh

$$\|\omega\|_{h,\infty}/\|\omega\|_\infty = a\mathrm{e}^{-(\gamma-\beta)t}\|\omega\|_{h,\infty}$$

for the moving grid calculations (solid). The fixed grid quantity with $N_1 = N_2 = 256$ is included as the dashed curve. Again, convergence is observed as $N$ is increased. The normalized maximum vorticity for the $N_1 = N_2 = 256$ calculation with moving grid is 0.9985 at $t = 1$.

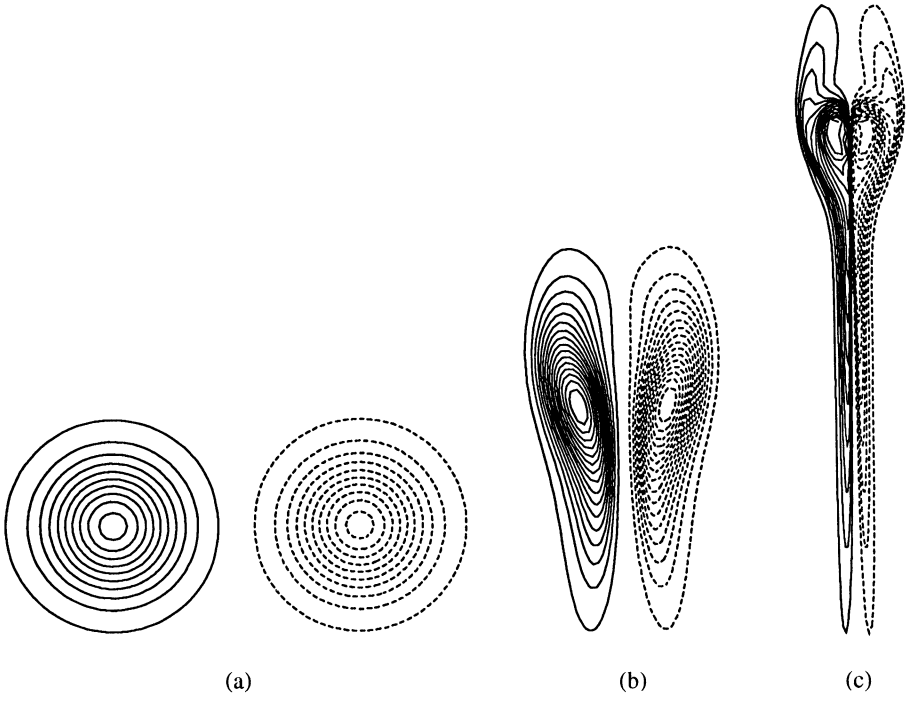



FIG. 7. *Contours of the vorticity for the two-vortex straining flow at* $t = 0, .5,$ *and* 1. *The contour levels in Fig.* 7(a) *from* $-9.4$ *to* 9.6, *in Fig.* 7(b) *from* $-16.3$ *to* 16.4, *and in Fig.* 7(c) *from* $-28.4$ *to* 28.5, *all with increments of* 1. *Here, the initial box size is* 4.2 *on a side,* $N_x = N_y = 256$, *and* $\Delta t = .00078125$.

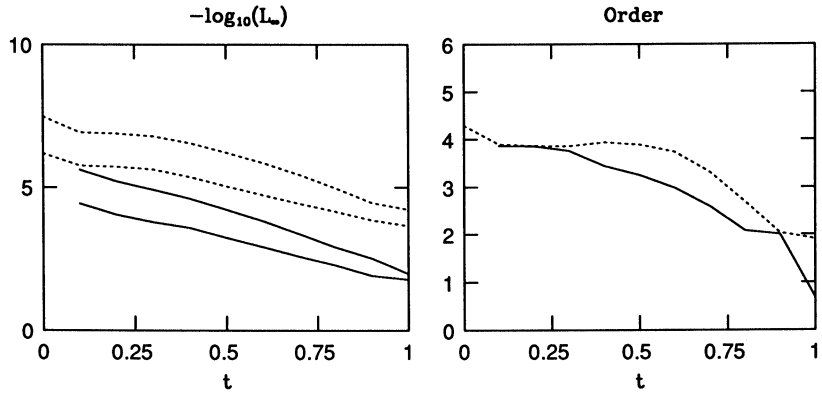



FIG. 8. *The approximated error in vorticity (solid) and velocity (dashed) with their orders in the right-hand box for* $N_x = N_y = 128, 256$. *The errors in vorticity are normalized by the maximum vorticity* $\|\omega\|_\infty(t) = a\exp(\gamma - \beta)t$. *The accuracy improves as N is increased. The right-hand box shows the orders of the computations.*

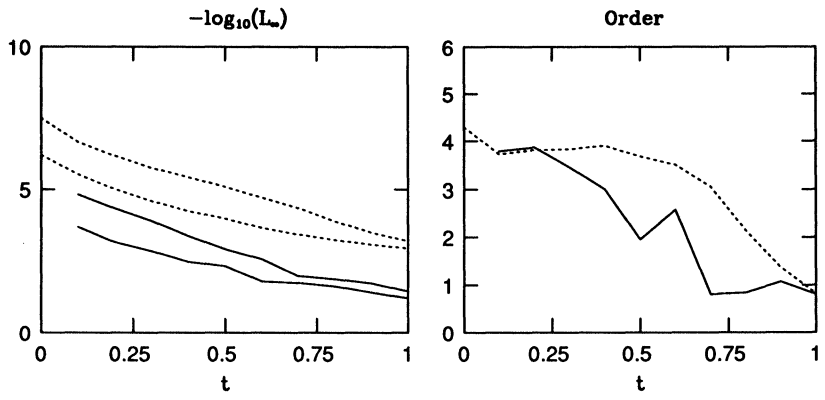



FIG. 9. *The same quantities as in Fig.* 7, *but with the initial grid held fixed.*

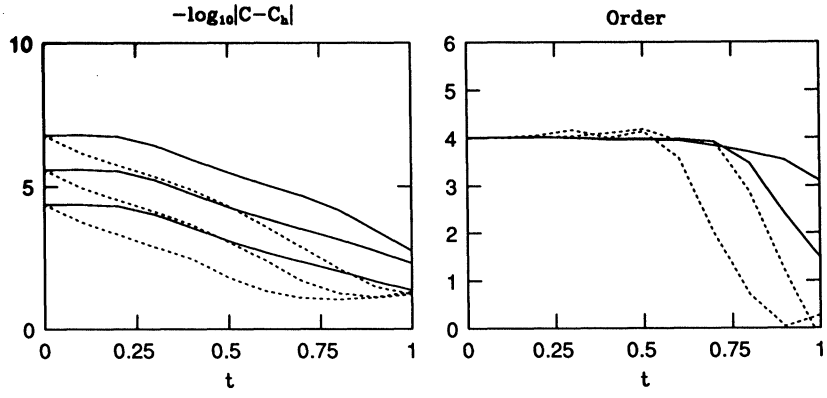



FIG. 10. *The circulation error in the right half-plane, with its approximation computed by using Simpson's rule in the right half-plane. The* solid *curves are for the* moving *grid and the* dashed *curves are for the* fixed *grid. The errors are for* $N_x = N_y = 64, 128, 256$. *The accuracy improves as N is increased. The order of these errors is presented in the right-hand box.*

Finally, we note that in recent work, Fishelov [15] also considered a fixed-grid method for the vorticity formulation of the two-dimensional, incompressible Euler equations. She used a vortex blob discretization evaluated by direct summation. This approach may be more useful for long times and for cases where the grid is allowed to move since the blob discretization provides improved stability for Lagrangian methods (see [5], for example). However, the blob approach is not likely to be useful for fixed grids and for short times, as we found that a vortex blob discretization with a Beale and Majda fourth-order kernel (using $\delta = h^{.95}$) gave velocity errors that were two orders of magnitude larger than those for our fourth-order modified point vortex discretization (2.12) at $t = 0$ and for the initial data (3.6) and $N_1 = N_2 = 256$.

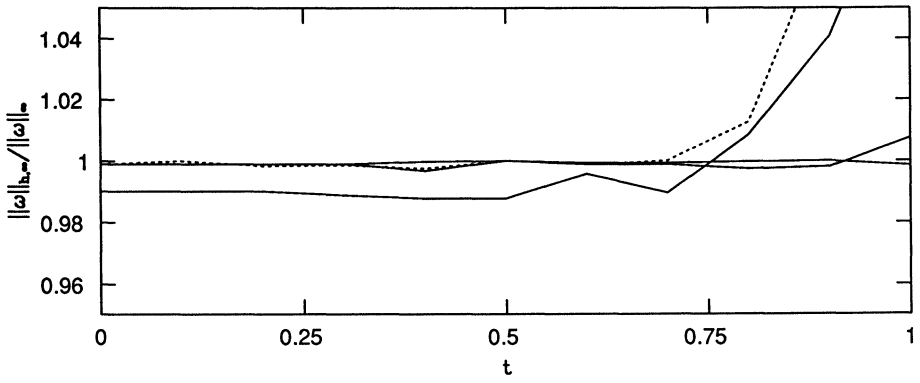



FIG. 11. *The normalized maximum vorticity on the grid,* $\|\omega\|_{h,\infty}/\|\omega\| = \alpha e^{-(\gamma-\beta)t}\|\omega\|_{h,\infty}$. *The* solid *curves are for the* moving *grid with* $N_x = N_y = 64, 128, 256$, *and the* dashed *curve is for the* fixed *grid with* $N_x = N_y = 256$. *The difference from* 1 *decreases as N is increased.*

**4. Conclusion.** In this work we have developed new numerical methods, based on the vorticity formulation, for solving the two-dimensional, incompressible Euler equations. In the vorticity formulation of the Euler equations, the velocity is obtained directly from the vorticity through the Biot–Savart integral, and the vorticity is updated on the computational grid. An advantage of this formulation for open and periodic problems is that asymptotic boundary conditions on the velocity are explicitly incorporated into the Biot–Savart kernel, and the focus is then simply on finding accurate and efficient methods for evaluating the Biot–Savart integral over a regular mesh. Here we have considered the point vortex approximation on rectangular meshes.

Using the Poisson summation formula generalized to include singular integrands, we constructed the explicit error expansion for the point vortex approximation to the Biot–Savart integral. The existence of the error expansion was proved by Goodman et al. more generally on smooth, curvilinear grids, but the method of proof was not constructive. Thus in the case of a rectangular grid, we have proved an explicit example of the expansion. We found that the leading second-order error term depends on the vorticity only through the local value of its gradient. The coefficient is expressible as a two-dimensional lattice sum, and we demonstrate how its calculation can be done easily and rapidly. This leads to a simple modification of the point vortex approximation that yields fourth-order accuracy. In the special case of a square grid, the method of lines formulation of the vorticity transport equation, using the unmodified, second-order point vortex approximation and a fourth-order gradient approximation, automatically yields a fourth-order evolution of the vorticity. We note also that in the square grid case, the error expansion contains terms with only fourth powers of $h$ after the leading second-order term.

Furthermore, we have demonstrated the utility of these methods through their employment to solve both the nonlinear roll-up of a thin, spatially periodic shear layer, and the interaction of two oppositely signed vortices being pushed together under an external, three-dimensional straining flow. As the summations were done on a rectangular grid, the FFT algorithm was used (through use of the discrete convolution theorem) to rapidly evaluate the velocity on the grid. Thus, the calculations are performed at high

resolution. We were able to accurately follow the evolution of the shear layer well into the nonlinear regime, where the bulk of the vorticity has concentrated itself into a central vortex. This concentration is linked, in the thin layer limit, to the formulation of singularities observed in vortex sheets [3]. By employing a grid that collapsed naturally with the external compressive flow, we were able to compute the motion of two vortices driven together under the strain. Physically, the interest lies in their severe deformation and elongation, which yields enhanced dissipation in the presence of viscosity (see, for example, [9] for viscous calculations).

These methods have already found application in the study of buoyancy-driven flows, including both two-dimensional Boussinesq and fully stratified fluids [25]. In both these cases, the incompressibility constraint gives the Biot–Savart relation between velocity and vorticity, and the methods are directly applicable. There are several other directions that further work should take. Our time integration method does not make use of the fact that the vorticity transport equation is a conservation law. The use of methods constructed for such transport equations, such as ENO methods [19], or other high-order Godunov type schemes, would improve the robustness of these methods (see also [7]). It would also be useful to find the second-order error coefficient for the point vortex approximation on a generally smooth, curvilinear coordinate system. This would allow the construction of fourth-order methods together with more general adaptivity, without resorting to explicit extrapolation to gain additional accuracy. For the three-dimensional Euler equations, we have seen that there is an apparent difficulty in directly applying the methods developed here to the so-called grid-free point vortex approximation. We are currently studying this. We note that the existence of asymptotic error expansions has been proved not only for the three-dimensional Biot–Savart integral, but also for its gradient whose computation is necessary to compute the stretching term in the vorticity transport equation (see [13]). Another very important extension is to devise methods to treat the presence of walls, both with and without the presence of viscosity.

**Appendix A. Poisson summation formula for singular functions.** In this appendix, we present a version of the usual Poisson summation formula (see [14], for example) extended to the case of a function with an isolated and integrable singularity at the origin and in two space dimensions. It will be clear from this analysis how to obtain more general results. We begin by introducing some notation.

Define the Fourier transform in two dimensions by

$$\hat{f}(\mathbf{k}) = \int_{-\infty}^{+\infty}\int_{-\infty}^{+\infty} e^{-i\mathbf{k}\cdot\mathbf{x}} f(\mathbf{x}) dx_1 dx_2, \tag{A.1}$$

where $\mathbf{k} = (k_1, k_2)$ and $\mathbf{x} = (x_1, x_2)$. Its inverse transform is given by

$$f(\mathbf{x}) = \frac{1}{(2\pi)^2}\int_{-\infty}^{+\infty}\int_{-\infty}^{+\infty} e^{-i\mathbf{k}\cdot\mathbf{x}} \hat{f}(\mathbf{x}) dk_1 dk_2. \tag{A.2}$$

Define the convolution of the functions $f, g$ by

$$f * g(\mathbf{x}) = \int_{-\infty}^{+\infty}\int_{-\infty}^{+\infty} f(\mathbf{x}-\mathbf{x}')g(\mathbf{x}')dx_1' dx_2'. \tag{A.3}$$

By the convolution theorem,

$$\widehat{f * g}(\mathbf{k}) = \hat{f}(\mathbf{k})\hat{g}(\mathbf{k}) \tag{A.4}$$

and

$$\widehat{fg}(\mathbf{k}) = \frac{1}{(2\pi)^2}\hat{f} * \hat{g}(\mathbf{k}). \tag{A.5}$$

Denote a smoothing function by $\delta_\epsilon(\mathbf{x})$, and let it satisfy the usual properties of an approximate identity [31]. Then for any $f$, a smoothed version of it is given by

$$f_\epsilon(\mathbf{x}) = f * \delta_\epsilon(\mathbf{x}). \tag{A.6}$$

Define the physical space grid by

(A.7)

$$\Lambda(\alpha_1, \alpha_2) = \{\mathbf{x_j} \,|\mathbf{x_j} = (j_1 h_1, j_2 h_2) \text{ with } h_1 = \alpha_1 h, h_2 = \alpha_2 h \quad \text{and} \quad \mathbf{j} = (j_1, j_2) \in \mathbf{Z}^2\},$$

and the dual phase space grid by

$$\Lambda^*(\alpha_1, \alpha_2) = \left\{\mathbf{k_j} \mid \mathbf{k_j} = \left(\frac{1}{\alpha_1} j_1, \frac{1}{\alpha_2} j_2\right) \quad \text{and} \quad \mathbf{j} = (j_1, j_2) \in \mathbf{Z}^2\right\}. \tag{A.8}$$

Then we obtain the following formula.

POISSON SUMMATION FORMULA FOR SINGULAR FUNCTIONS. *Let $f(\mathbf{x})$ be rapidly decaying in $\mathbf{x}$, and smooth except for an isolated and integrable singularity at $\mathbf{x} = \mathbf{0}$. Then,*

$$\sum_{\mathbf{x}\in\Lambda(\alpha_1,\alpha_2)\setminus\mathbf{0}} f(\mathbf{x_j}) h_1 h_2 - \int_{-\infty}^{+\infty}\int_{-\infty}^{+\infty} f(\mathbf{x}) dx_1 dx_2 = \lim_{\epsilon\to 0}\left[\sum_{\mathbf{k_j}\in\Lambda^*(\alpha_1,\alpha_2)\setminus\mathbf{0}} \hat{f}_\epsilon\left(\frac{2\pi}{h}\mathbf{k_j}\right) - f_\epsilon(\mathbf{0}) h_1 h_2\right], \tag{A.9}$$

*where $f_\epsilon$ is the smoothed version of $f$.*

*Remark* 1. As the function $f$ has a singularity at the origin, its Fourier coefficients may decay too slowly to be absolutely summable. Consequently, the smoothing function $\delta_\epsilon(\mathbf{x})$ provides the mechanism to interpret their sum. In addition, the smoothing also gives rise to a residue, or self-induction term. However, since the left-hand side of (A.9) is independent of the choice of smoothing function, so is the right-hand side. Thus all smoothing effects in it must cancel.

*Remark* 2. Under certain circumstances, depending on the function $f$ *and* the smoothing function $\delta_\epsilon$, the limit of the right-hand side of (A.9) exists for each term separately. We discuss this in detail after the proof.

*Remark* 3. Equation (A.9) can be generalized to functions with nonintegrable singularities provided they can be interpreted in the principle value sense. In this case, the choice of smoothing functions is restricted to the ones that give the correct principle value in the continuous case, i.e., in the integral on the left-hand side of (A.9) is replaced by

$$\text{P.V.} \int_{-\infty}^{+\infty}\int_{-\infty}^{+\infty} f(\mathbf{x}) dx_1 dx_2,$$

while the rest of the formula (A.9) remains unchanged.

*Remark* 4. The formula (A.9) can also be generalized to functions with several isolated singularities. For example, suppose that the singular points are $\mathbf{z}_1, \ldots, \mathbf{z}_n$. Let the

smoothed version of $f$ be $f_\epsilon$ as before. If the singular points lie on the grid $\Lambda(\alpha_1, \alpha_2)$, then (A.9) becomes

$$\sum_{\substack{\mathbf{x_j}\in\Lambda(\alpha_1,\alpha_2)\\ \mathbf{x_j}\neq z_1,\ldots,z_n}} f(\mathbf{x_j})h_1h_2 - \int\int f(\mathbf{x})dx_1dx_2 = \lim_{\epsilon\to 0}\left[\sum_{\mathbf{k_j}\in\Lambda^*(\alpha_1,\alpha_2)\setminus\mathbf{0}} \hat{f}_\epsilon\left(\frac{2\pi}{h}\mathbf{k_j}\right) - \sum_{l=1}^{n} f_\epsilon(\mathbf{z}_l)h_1h_2\right]. \tag{A.10}$$

*Proof of summation formula.* The proof of (A.9) is almost trivial. We rely on the Poisson summation formula for smooth functions [12] as stated in the following.

POISSON SUMMATION FOR SMOOTH FUNCTIONS. *Let $g(\mathbf{x})$ be smooth and rapidly decaying. Then,*

$$\sum_{\mathbf{x_j}\in\Lambda(\alpha_1,\alpha_2)} g(\mathbf{x_j})h_1h_2 - \int_{-\infty}^{+\infty}\int_{-\infty}^{+\infty} g(\mathbf{x})dx_1dx_2 = \sum_{\mathbf{k_j}\in\Lambda^*(\alpha_1,\alpha_2)\setminus\mathbf{0}} \hat{g}\left(\frac{2\pi}{h}\mathbf{k_j}\right). \tag{A.11}$$

Now we apply this formula to $f_\epsilon$, which is the smoothed version of $f$. Thus, we have

$$\sum_{\mathbf{x_j}\in\Lambda(\alpha_1,\alpha_2)} f_\epsilon(\mathbf{x_j})h_1h_2 - \int_{-\infty}^{+\infty}\int_{-\infty}^{+\infty} f_\epsilon(\mathbf{x})dx_1dx_2 = \sum_{\mathbf{k_j}\in\Lambda^*(\alpha_1,\alpha_2)\setminus\mathbf{0}} \hat{f}_\epsilon\left(\frac{2\pi}{h}\mathbf{k_j}\right). \tag{A.12}$$

Now write

$$\sum_{\mathbf{x_j}\in\Lambda(\alpha_1,\alpha_2)} f_\epsilon(\mathbf{x_j})h_1h_2 = \sum_{\mathbf{x_j}\in\Lambda(\alpha_1,\alpha_2)\setminus\mathbf{0}} f_\epsilon(\mathbf{x_j})h_1h_2 + f_\epsilon(\mathbf{0})h_1h_2. \tag{A.13}$$

Therefore, we get

$$\sum_{\mathbf{x_j}\in\Lambda(\alpha_1,\alpha_2)\setminus\mathbf{0}} f_\epsilon(\mathbf{x_j})h_1h_2 - \int_{-\infty}^{+\infty}\int_{-\infty}^{+\infty} f_\epsilon(\mathbf{x})dx_1dx_2 = \sum_{\mathbf{k_j}\in\Lambda^*(\alpha_1,\alpha_2)\setminus\mathbf{0}} \hat{f}_\epsilon\left(\frac{2\pi}{h}\mathbf{k_j}\right) - f_\epsilon(\mathbf{0})h_1h_2. \tag{A.14}$$

The limit as $\epsilon \to 0$ of the left-hand side of (A.14) clearly exists. Consequently, the limit as $\epsilon \to 0$ of the right-hand side exists and yields the result (A.9).

It is natural here to address the question of whether the limit of the right-hand side of (A.9) can be taken for each term separately. It is sufficient to determine whether the limit as $\epsilon \to 0$ of $f_\epsilon(\mathbf{0})$ exists. If it does, the existence of the limit of the left-hand side of (A.9) implies that the limit of the sum of Fourier coefficients must then also exist and hence the limit can be separated.

Suppose that $f(\mathbf{x})$ can be written as

$$f(\mathbf{x}) = H(\mathbf{x})g(\mathbf{x}), \tag{A.15}$$

where $H(\mathbf{x})$ contains the local singularity and $g(\mathbf{x})$ is smooth and rapidly decaying. Then we have

$$f_\epsilon(\mathbf{0}) \int_{-\infty}^{+\infty}\int_{-\infty}^{+\infty} H(\mathbf{x})g(\mathbf{x})\delta_\epsilon(\mathbf{x})dx_1dx_2. \tag{A.16}$$

Define a characteristic function $\chi_R$ by

$$\chi_R(\mathbf{x}) = \begin{cases} 1 \text{ if } |x_1| \le R \text{ and } |x_2| \le R, \\ 0 \text{ otherwise}. \end{cases} \tag{A.17}$$

Furthermore, define $\tilde{g}(\mathbf{x})$ by

$$\tilde{g}(\mathbf{x}) = g(\mathbf{x}) - [g(\mathbf{0}) + \nabla g(\mathbf{0}) \cdot \mathbf{x}]\chi_R(\mathbf{x}). \tag{A.18}$$

Then $f_\epsilon(\mathbf{0})$ becomes

$$\begin{aligned} f_\epsilon = g(\mathbf{0}) &\int_{-\infty}^{+\infty}\int_{-\infty}^{+\infty} H(\mathbf{x})\delta_\epsilon(\mathbf{x})\chi_R(\mathbf{x})dx_1dx_2 \\ &+\nabla g(\mathbf{0}) \cdot \int_{-\infty}^{+\infty}\int_{-\infty}^{+\infty} \mathbf{x}H(\mathbf{x})\delta_\epsilon(\mathbf{x})\chi_R(\mathbf{x})dx_1dx_2 \\ &+\int_{-\infty}^{+\infty}\int_{-\infty}^{+\infty} H(\mathbf{x})\tilde{g}(\mathbf{x})\delta_\epsilon(\mathbf{x})dx_1dx_2 \\ \equiv I_{\epsilon,R} &+ II_{\epsilon,R} + III_{\epsilon,R}. \end{aligned} \tag{A.19}$$

Since $H(\mathbf{x}), \mathbf{x}H(\mathbf{x})$, and $H(\mathbf{x})\tilde{g}(\mathbf{x})$ have successively smoother behavior as $|\mathbf{x}| \to 0$, there is no hope for cancellation of divergent terms by summing the different integrals. Therefore, the limit as $\epsilon \to 0$ of $f_\epsilon(\mathbf{0})$ exists if and only if the limit as $\epsilon \to 0$ of $I_{\epsilon,R}$, $II_{\epsilon,R}$, and $III_{\epsilon,R}$ exists separately.

Consider $I_{\epsilon,R}$ first.

$$\lim_{\epsilon\to 0} I_{\epsilon,R} = \lim_{\epsilon\to 0}\int_{-R}^{+R}\int_{-R}^{+R} H(\mathbf{x})\delta_\epsilon(\mathbf{x})dx_1dx_2. \tag{A.20}$$

Since $H(\mathbf{x})$ has a local singularity at the origin, the only way such a limit can exist is by some cancellation. Therefore, suppose that

$$H(\mathbf{x}) = -H(-\mathbf{x}), \qquad \delta_\epsilon(\mathbf{x}) = \delta_\epsilon(-\mathbf{x}). \tag{A.21}$$

Then, $I_{\epsilon,R} = 0$ for any $\epsilon$ and $R$ and hence the limit (A.20) exists and is equal to 0.

Consider $III_{\epsilon,R}$ next. By construction, $H(\mathbf{x})\tilde{g}(\mathbf{x}) = O(|\mathbf{x}|)$ as $|\mathbf{x}| \to 0$ and is integrable. Therefore,

$$\lim_{\epsilon\to 0} III_{\epsilon,R} = \lim_{\epsilon\to 0}\int_{-\infty}^{+\infty}\int_{-\infty}^{+\infty} H(\mathbf{x})\tilde{g}(\mathbf{x})\delta_\epsilon(\mathbf{x})dx_1dx_2 = 0 \tag{A.22}$$

by standard arguments such as the Riemann–Lebesgue lemma if $\delta_\epsilon$ is the Dirichlet kernel (see below).

Finally, it remains to consider $II_{\epsilon,R}$. The existence of this limit is a classical question in harmonic analysis. In general, this limit will exist if and only if $\mathbf{x} = \mathbf{0}$ is a Lebesgue or a Dirichlet point (see [30]) of the function $\mathbf{x}H(\mathbf{x})$. We do not give the most generally known conditions for the existence of such points here, but it is easy to show that if $H(\mathbf{x}) = K_i(\mathbf{x})$ then these limits exist. $K_1$ with $i = 1, 2$ denotes the components of the Biot–Savart kernel.

For simplicity, we consider two standard types of smoothing functions: scaled and dilated $L^1$ functions

$$\delta_\epsilon(\mathbf{x}) = \frac{1}{\epsilon^2}\eta\left(\frac{x_1}{\epsilon}, \frac{x_2}{\epsilon}\right) \tag{A.23}$$

with $\eta$ even, positive, and of mean 1, and the Dirichlet kernel

$$\delta_\epsilon(\mathbf{x}) = \delta_{\frac{1}{M}}(\mathbf{x}) = \frac{\sin\left(\frac{Mx_1}{\alpha_1}\right)}{\pi x_1}\frac{\sin\left(\frac{Mx_2}{\alpha_2}\right)}{\pi x_2}, \tag{A.24}$$

where $\alpha_1, \alpha_2$ serve to weight the coordinate directions (see Appendix C).

Now correspondingly, write $II_{\epsilon,R}$ as $II^s_{\epsilon,R}$ for the scaled smoothing function

$$II^s_{\epsilon,R} = \int_{-\frac{R}{\epsilon}}^{+\frac{R}{\epsilon}}\int_{-\frac{R}{\epsilon}}^{+\frac{R}{\epsilon}} \tilde{\mathbf{H}}(\epsilon\mathbf{x})\eta(\mathbf{x})dx_1dx_2, \tag{A.25}$$

where $\tilde{\mathbf{H}}(\mathbf{x}) = \mathbf{x}H(\mathbf{x})$, and as $II^D_{\epsilon,R}$ for the Dirichlet kernel

$$II^D_{\frac{1}{M},R} = \frac{1}{\pi^2}\int_{-\frac{RM}{\alpha_2}}^{+\frac{RM}{\alpha_2}}\int_{-\frac{RM}{\alpha_1}}^{+\frac{RM}{\alpha_1}} \tilde{\mathbf{H}}\left(\frac{\alpha_1 x_1}{M}, \frac{\alpha_2 x_2}{M}\right)\frac{\sin(x_1)}{x_1}\frac{\sin(x_2)}{x_2}dx_1dx_2. \tag{A.26}$$

The question reduces to whether the limit as $\epsilon \to 0$ exists for $II^s_{\epsilon,R}$ or $II^D_{\epsilon,R}$. Now take $H(\mathbf{x}) = \mathbf{K}_i(\mathbf{x})$. Then notice that with this choice, $\tilde{\mathbf{H}}(\mathbf{x})$ is homogeneous of degree 0 so that

$$II^s_{\epsilon,R} = \int_{-\frac{R}{\epsilon}}^{+\frac{R}{\epsilon}}\int_{-\frac{R}{\epsilon}}^{+\frac{R}{\epsilon}} \tilde{\mathbf{H}}(\mathbf{x})\eta(\mathbf{x})dx_1dx_2 \tag{A.27}$$

and

$$II^D_{\frac{1}{M},R} = \frac{1}{\pi^2}\int_{-\frac{RM}{\alpha_2}}^{+\frac{RM}{\alpha_2}}\int_{-\frac{RM}{\alpha_1}}^{+\frac{RM}{\alpha_1}} \tilde{\mathbf{H}}(\alpha_1 x_1, \alpha_2 x_2)\frac{\sin(x_1)}{x_1}\frac{\sin(x_2)}{x_2}dx_1dx_2. \tag{A.28}$$

It is clear that the limit as $\epsilon \to 0$ of $II^s_{\epsilon,R}$ exists since $\tilde{\mathbf{H}}(\mathbf{x})$ is bounded on the plane and $\eta \in L^1(\mathbf{R}^2)$. The limit as $M \to \infty$ of $II^D_{\frac{1}{M},R}$ is directly calculable by contour integration (see Appendix C). Consequently, the limit of the right-hand side of (A.9) can be separated as follows.

SPECIAL POISSON SUMMATION FORMULA FOR THE BIOT–SAVART KERNEL. *If $f(\mathbf{x}) = K_i(\mathbf{x})g(\mathbf{x})$, $g$ is smooth and rapidly decaying, and $\delta_\epsilon$ is either the scaled smoothing function or the Dirichlet kernel, then*

$$\begin{aligned}&\sum_{\mathbf{x_j}\in\Lambda(\alpha_1,\alpha_2)\setminus\mathbf{0}} f(\mathbf{x_j})h_1h_2 - \int_{-\infty}^{+\infty}\int_{-\infty}^{+\infty} f(\mathbf{x})dx_1dx_2 = \\ &\text{P.V.}\sum_{\mathbf{k_j}\in\Lambda^*(\alpha_1,\alpha_2)\setminus\mathbf{0}} \hat{f}\left(\frac{2\pi}{h}\mathbf{k_j}\right) - \lim_{\epsilon\to 0} f_\epsilon(\mathbf{0})h_1h_2,\end{aligned} \tag{A.29}$$

*where the* P.V. *denotes the principal value sum defined by*

$$\text{P.V.}\sum_{\mathbf{k}_j\in\Lambda(\alpha_1,\alpha_2)\setminus\mathbf{0}} \hat{f}\left(\frac{2\pi}{h}\mathbf{k_j}\right) = \lim_{\epsilon\to 0}\sum_{\mathbf{k}_j\in\Lambda(\alpha_1,\alpha_2)\setminus\mathbf{0}} \hat{f}\left(\frac{2\pi}{h}\mathbf{k_j}\right). \tag{A.30}$$

*Remark* 1. We use this formula (A.29) with $g(\mathbf{x}) = \omega(\mathbf{x})$ in Appendices B and C to construct the explicit error expansion.

*Remark* 2. Although the result (A.29) is independent of the smoothing function, the rate of convergence as $\epsilon \to 0$ is highly dependent on the choice. In Appendix C, we exploit this property by using the Dirichlet kernel as the smoothing function. This yields rapidly and absolutely convergent sums and thus enables us to obtain very accurate approximations of error expansion coefficients.

*Remark* 3. Of course, the formula (A.29) holds for more general functions $f = Hg$. Generally, if the limit as $\epsilon \to 0$ of $I_{\epsilon,R}$, $II_\epsilon$, $R$, and $III_{\epsilon,R}$ exists, then (A.29) holds, although even this is not the most general case. Notice, though, that the three-dimensional version of $II_{\epsilon,R}$ does not have a limit since there the Biot–Savart kernel is $O(1/|x|^2)$ as $|x| \to 0$ so that the corresponding $\mathbf{x}H(\mathbf{x})$ is unbounded at the origin. This is currently under study.

**Appendix B. Error Expansion.** In this appendix we obtain an error expansion for the point vortex approximation to the Biot–Savart integral on a rectangular mesh. The expansion is obtained through an asymptotic analysis of the Fourier coefficients appearing in the special Poisson formula for the Biot–Savart kernel (A.29).

In previous work, Goodman, Hou, and Lowengrub [16] proved the existence of such an error expansion. However, it is difficult to determine the coefficients of the expansion from their method of proof. For example, their second-order coefficient contains an undetermined constant of integration. Our proof is similar to theirs in spirit, but our method provides a prescription for the explicit determination of the coefficients.

In this appendix, we do not derive explicit expressions for the coefficients, although we indicate how it is done. We save their explicit evaluation for Appendix C where we obtain an expression for the second-order coefficient. This term is the most delicate to obtain. The Biot–Savart kernel in two dimensions is

$$\mathbf{K}(\mathbf{x}) = \frac{1}{2\pi}\frac{(-x_2, x_1)}{{x_1}^2 + {x_2}^2}, \tag{B.1}$$

where $\mathbf{x} = (x_1, x_2)$. We want to describe the discretization error between the Biot–Savart integral and the point vortex approximation

$$\int_{-\infty}^{+\infty}\int_{-\infty}^{+\infty} \mathbf{K}(\mathbf{x_l} - \mathbf{x})\omega(\mathbf{x})dx_1dx_2 - \sum_{\mathbf{x_j}\in\Lambda(\alpha_1,\alpha_2)\setminus\mathbf{x_l}} \mathbf{K}(\mathbf{x_l} - \mathbf{x_j})\omega(\mathbf{x_j})h_1h_2, \tag{B.2}$$

where $\Lambda(\alpha_1, \alpha_2)$ is the rectangular grid defined in (A.7), $h_1 = \alpha_1 h$ and $h_2 = \alpha_2 h$.

It would be routine to describe this error if the integrand were smooth. However, $\mathbf{K}(\mathbf{x})$ has an isolated integrable singularity at $\mathbf{x} = \mathbf{0}$. Thus, to handle this, we use the special Poisson summation formula (A.29).

Without loss of generality, and for the sake of clarity, we study the error $\mathbf{I}(\mathbf{0}) - \mathbf{I}_h(\mathbf{0})$, where

$$\mathbf{I}(\mathbf{0}) = \int_{-\infty}^{+\infty}\int_{-\infty}^{+\infty} \mathbf{K}(\mathbf{x})\omega(\mathbf{x})dx_1dx_2 \tag{B.3}$$

and

$$\mathbf{I}_h(\mathbf{0}) = \sum_{\mathbf{x_j}\in\Lambda(\alpha_1,\alpha_2)\setminus\mathbf{0}} \mathbf{K}(\mathbf{x_j})\omega(\mathbf{x_j})h_1h_2. \tag{B.4}$$

This corresponds to taking $\mathbf{x}_1 = \mathbf{0}$ in (B.2) and dropping the minus sign inside the kernel. Now, following the prescription of Appendix A, w define the smoothed version of the integrand in (B.3) by

$$(\mathbf{K}\omega)_\epsilon(\mathbf{x}) = (\mathbf{K}\omega) * \delta_\epsilon(\mathbf{x}) = \int_{-\infty}^{+\infty}\int_{-\infty}^{+\infty} \mathbf{K}(\mathbf{x}')\omega(\mathbf{x}')\delta_\epsilon(\mathbf{x}-\mathbf{x}')dx_1'dx_2', \tag{B.5}$$

where $\delta_\epsilon(\mathbf{x})$ is given by (A.23) or (A.24).

The purpose of this section is now to prove the following result.

THEOREM 1 POINT VORTEX ERROR EXPANSION. *For $\omega(\mathbf{x})$ smooth and rapidly decaying, there exist coefficients $\tilde{\mathbf{C}}(\alpha)[\omega]_{\mathbf{0},2n}$ such that*

$$\mathbf{I}(\mathbf{0}) - \mathbf{I}_h(\mathbf{0}) = \lim_{\epsilon\to 0}(\mathbf{K}\omega)\,\epsilon(\mathbf{0})h_1h_2 + \sum_{n=1}^{N-1}\left(\frac{h}{2\pi}\right)^{2n}\tilde{C}(\alpha)[\omega]_{\mathbf{0},2N} + O(h^{2N}) \tag{B.6}$$

*for any $N$, $\alpha$ is the grid aspect ratio $\alpha_1/\alpha_2$. Furthermore, the coefficients $\tilde{C}$ are given by*

$$\tilde{\mathbf{C}}(\alpha)[\omega]_{\mathbf{0},2n} = \sum_{\substack{r,q\\ r+q=2n-1}}\left(-D^{r,q}(\alpha)[\omega](\mathbf{0}), D^{q,r}\left(\frac{1}{\alpha}\right)[\omega](\mathbf{0})\right), \tag{B.7}$$

*and $D^{r,q}(\alpha)$ is a linear differential operator of order $r$ in $x_1$ and $q$ in $x_2$ and whose coefficients depend on $\alpha, r, q$.*

*Remark* 1. For $n > 1$, these coefficients are the coefficients shown in (2.6) and (2.13) of §2. The second-order term $\mathbf{C}(\alpha)[\omega]_{\mathbf{0},2}$ in (2.8a) differs from $\tilde{\mathbf{C}}(\alpha)[\omega]_{\mathbf{0},2}$ exactly by the self-induction term in (B.6).

*Remark* 2. Our method of proof relies on the application of the special Poisson summation formula for the Biot–Savart kernel (A.29), asymptotics of the resulting Fourier lattice sums, and controlling the error from the asymptotics. The method is very general and can be applied in many other contexts where singular integrals arise.

*Proof.* We begin with the following lemma.

DISCRETIZATION LEMMA. *Suppose that $\omega(\mathbf{x})$ is smooth and rapidly decaying. Then the discretization error $\mathbf{I}(\mathbf{0}) - \mathbf{I}_h(\mathbf{0})$ is given by*

$$\mathbf{I}(\mathbf{0}) - \mathbf{I}_h(\mathbf{0}) = \lim_{\epsilon\to 0}(\mathbf{K}\omega)_\epsilon(\mathbf{0})h_1h_2 - \text{P.V.}\sum_{\mathbf{l_j}\in\Lambda^*(\alpha_1,\alpha_2)\setminus\mathbf{0}}\widehat{\mathbf{K}\omega}\left(\frac{2\pi}{h}\mathbf{l_j}\right), \tag{B.8}$$

*where*

$$\text{P.V.}\sum_{\mathbf{l_j}\in\Lambda^*(\alpha_1,\alpha_2)\setminus\mathbf{0}}\widehat{\mathbf{K}\omega}\left(\frac{2\pi}{h}\mathbf{l_j}\right) = \lim_{\epsilon\to 0}\sum_{\mathbf{l_j}=\in\Lambda^*(\alpha_1,\alpha_2)\setminus\mathbf{0}}\widehat{\mathbf{K}\omega}\left(\frac{2\pi}{h}\mathbf{l_j}\right)\hat{\delta}_\epsilon\left(\frac{2\pi}{h}\mathbf{l_j}\right). \tag{B.9}$$

The proof of this lemma is a straightforward application of (A.29) with $\mathbf{f}_\epsilon = (\mathbf{K}\omega)_\epsilon$.

Thus, to determine the error expansion, we must now examine the lattice sum that appears on the right-hand side of (B.8).

Define the function

$$\mathbf{F}(l_1,l_2,m_1,m_2,\tau) = (F_1,F_2) = \frac{(-l_2+m_2\tau, l_1-m_1\tau)}{(l_1-m_1\tau)^2+(l_2-m_2\tau)^2} \tag{B.10}$$

with $\tau = \frac{h}{2\pi}$ as a small parameter. We now use $\mathbf{F}$ to evaluate $\widehat{\mathbf{K}\omega}(\frac{2\pi}{h}\mathbf{l})$ as follows.

LEMMA. *The Fourier transform of* $\mathbf{K}\omega$ *is*

$$\widehat{\mathbf{K}\omega}\left(\frac{2\pi}{h}\mathbf{l}\right) = \frac{-i}{(2\pi)^2}\tau \int_{-\infty}^{+\infty}\int_{-\infty}^{+\infty} \mathbf{F}(l_1, l_2, m_1, m_2, \tau)\hat{\omega}(\mathbf{m})dm_1, dm_2, \tag{B.11}$$

*where* $\tau = \frac{h}{2\pi}$.

*Proof.* Direct calculation gives

$$\hat{\mathbf{K}}(\mathbf{l}) = -i\frac{(-l_2, l_1)}{l_1^2 + l_2^2} \tag{B.12}$$

with $\mathbf{l} = (l_1, l_2)$. Now, by the convolution theorem, we get

$$\widehat{\mathbf{K}\omega}(\mathbf{l}) = \frac{1}{(2\pi)^2}\int_{-\infty}^{+\infty}\int_{-\infty}^{+\infty} \hat{\mathbf{K}}(\mathbf{l}-\mathbf{m})\hat{\omega}(\mathbf{m})dm_1 dm_2. \tag{B.13}$$

Then, combining (B.12), (B.13), and (B.10) gives the result (B.11).

Now, using the result (B.11) in (A.9), we get

$$\begin{aligned}\text{P.V.} \sum_{\mathbf{l_j}\in\Lambda^*(\alpha_1,\alpha_2)\setminus\mathbf{0}} \widehat{\mathbf{K}\omega}\left(\frac{2\pi}{h}\mathbf{l_j}\right) &= -\tau \lim_{\epsilon\to 0} \sum_{\mathbf{l_j}\in\Lambda^*(\alpha_1,\alpha_2)\setminus\mathbf{0}} \hat{\delta}_\epsilon\left(\frac{\mathbf{l_j}}{\tau}\right)\frac{i}{(2\pi)^2} \\ &\cdot \int_{-\infty}^{+\infty}\int_{-\infty}^{+\infty} \mathbf{F}(l_{j,1}, l_{j,2}, m_1, m_2, \tau)\hat{\omega}(\mathbf{m})dm_1 dm_2,\end{aligned} \tag{B.14}$$

where $\mathbf{l_j} = (l_{j,1}, l_{j,2})$. Thus, we need to consider the integral

$$\frac{i}{(2\pi)^2}\int_{-\infty}^{+\infty}\int_{-\infty}^{+\infty} \mathbf{F}(l_1, l_2, m_1, m_2, \tau)\hat{\omega}(\mathbf{m})dm_1, dm_2, \tag{B.15}$$

where $\mathbf{l} \in \Lambda^*(\alpha_1, \alpha_2)\setminus\mathbf{0}$. As $\tau$ is a small parameter, we want to expand (B.15) in $\tau$ (recall that $\tau = h/2\pi$). It is this expansion that, combined with the self-induction term, yields the error expansion. Of course, the function $\mathbf{F}$ has a singularity, and so we must be careful how we do this.

FOURIER LATTICE SUM EXPANSION LEMMA. *Suppose that* $\omega(\mathbf{x})$ *is smooth and rapidly decaying, and define* $\alpha$ *to be the aspect ratio of the grid* $\alpha = \alpha_1/\alpha_2$. *Then we obtain the following expansion for the Fourier lattice sum* (B.14):

$$\text{P.V.} \sum_{\mathbf{l_j}\in\Lambda^*(\alpha_1,\alpha_2)\setminus\mathbf{0}} \widehat{\mathbf{K}\omega}\left(\frac{2\pi}{h}\mathbf{l_j}\right) = \sum_{n=1}^{N-1}\left(\frac{h}{2\pi}\right)^{2n} \tilde{\mathbf{C}}(\alpha)[\omega]_{\mathbf{0},2n} + O(h^{2n}) \tag{B.16}$$

*for any* $N$, *where*

$$\tilde{\mathbf{C}}(\alpha)[\omega]_{\mathbf{0},2n} = \sum_{\substack{r,q \\ r+q=2n-1}} \left(-D^{r,q}(\alpha)[\omega](\mathbf{0}), D^{q,r}\left(\frac{1}{\alpha}\right)[\omega](\mathbf{0})\right), \tag{B.17}$$

*and* $D^{r,q}(\alpha)$ *is a linear differential operator of order* $r$ *in* $x_1$ *and* $q$ *in* $x_2$ *whose coefficients depend on* $\alpha, r, q$.

*Remark* 1. As we will see, the differential operators $D^{r,q}$ arise because an expansion of $\mathbf{F}$ in (B.15) leads to the calculation of moments of $\hat{\omega}$. These moments are then identified with the derivatives of $\omega$.

*Remark* 2. Although the coefficients $\tilde{\mathbf{C}}(\alpha)[\omega]_{\mathbf{0},2n}$ depend on principle value lattice sums, only the value of the second-order term ($n = 1$) will change according to the smoothing function. This term involves a lattice sum that is not absolutely summable and thus its value will depend on how it is summed. For $n > 1$, there is no ambiguity in how the sum is taken as the relevant lattice sums are absolutely convergent.

*Remark* 3. As a result of the special sensitivity of the second-order term, we will discuss it in more detail in Appendix C. In particular, we will see how its value depends on the type of smoothing. Of course, as the resulting expansion is independent of the smoothing function, the self-induction term compensates for the dependence on the smoothing function here. This is analogous to the undetermined constant of integration in the analysis of Goodman, Hou, and Lowengrub [16].

*Remark* 4. The symmetry of the coefficients $\tilde{\mathbf{C}}$ in $\alpha$ and $r, q$ is a result of the relationship between $F_1$ and $F_2$, i.e., $F_2(l_1, l_2, m_1, m_2, \tau) = -F_1(l_2, l_1, m_2, m_1, \tau)$.

*Remark* 5. In the square grid case $\alpha = 1$, it can be shown that $\tilde{\mathbf{C}}(\alpha)[\omega]_{\mathbf{0},2n} = \mathbf{0}$ for $n$ odd. Thus, but for the second-order term, expansion is in powers of $h^4$. We do not present this here.

*Proof.* We begin by examining $\mathbf{F}$. Notice that $\mathbf{F}$ has a singular point at

$$(m_1, m_2) = \left(\frac{l_1}{\tau}, \frac{l_2}{\tau}\right). \tag{B.18}$$

Thus, since $\tau$ is a small parameter, we can expand $\mathbf{F}$ away from the singular point (B.18) in a series about $\tau = 0$:

$$\mathbf{F}(l_1, l_2, m_1, m_2, \tau) = \sum_{n=0}^{\infty} \partial_\tau^n \mathbf{F}(l_1, l_2, m_1, m_2, 0) \frac{\tau^n}{n!}. \tag{B.19}$$

We define a box in $\mathbf{m}$-space about the singular point (B.18) by

$$\mathbf{B} = \left[\frac{l_1 - \tau}{\tau}, \frac{l_1 + \tau}{\tau}\right] \times \left[\frac{l_2 - \tau}{\tau}, \frac{l_2 + \tau}{\tau}\right]. \tag{B.20}$$

Then, consider the integral (B.15):

$$\begin{aligned} &\frac{i}{(2\pi)^2} \int_{-\infty}^{+\infty} \int_{-\infty}^{+\infty} \mathbf{F}(l_1, l_2, m_1, m_2, \tau) \hat{\omega}(\mathbf{m}) dm_1 dm_2 \\ &= \frac{i}{(2\pi)^2} \int\int_{\mathbf{R}^2 \setminus B} \mathbf{F}(l_1, l_2, m_1, m_2, \tau) \hat{\omega}(\mathbf{m}) dm_1 dm_2 \\ &\quad + \frac{i}{(2\pi)^2} \int\int_{B} \mathbf{F}(l_1, l_2, m_1, m_2, \tau) \hat{\omega}(\mathbf{m}) dm_1 dm_2 \\ &\equiv I + II. \end{aligned} \tag{B.21}$$

Now, the expansion (B.19) of $\mathbf{F}$ can be used in $I$. We will show later that $II$ is of arbitrarily high order in $\tau = (h/2\pi)$. Using the expansion, we write $I$ as

$$I = \sum_{n=0}^{\infty} \frac{\tau^n}{n!} \frac{i}{(2\pi)^2} \int\int_{\mathbf{R}^2 \setminus B} \partial_\tau^n \mathbf{F}(l_1, l_2, m_1, m_2, 0) \hat{\omega}(\mathbf{m}) dm_1 dm_2. \tag{B.22}$$

Furthermore, we notice that $\partial_\tau^n \mathbf{F}(l_1, l_2, m_1, m_2, 0)$ is separable. That is, in each component of $\mathbf{F}$, we can separate the $\mathbf{l}$ and $\mathbf{m}$ dependence as follows:

$$\frac{i}{(2\pi)^2} \partial_\tau^n F_1(l_1, l_2, m_1, m_2, 0) = \frac{i}{(2\pi)^2} \sum_{\substack{r,q \\ r+q=n}} c_1^{r,q}(l_1, l_2) m_1^r m_2^q \tag{B.23}$$

and

$$\begin{aligned}\frac{i}{(2\pi)^2}\partial_r^n F_2(l_1,l_2,m_1,m_2,0) &= \frac{i}{(2\pi)^2}\sum_{\substack{r,q\\ r+q=n}} c_2^{r,q}(l_1,l_2)m_1^r m_2^q \\ &= -\frac{i}{(2\pi)^2}\sum_{\substack{r,q\\ r+q=n}} c_1^{r,q}(l_2,l_1)m_2^r m_1^q \\ &= -\frac{i}{(2\pi)^2}\sum_{\substack{r,q\\ r+q=n}} c_1^{r,q}(l_2,l_1)m_1^q m_2^r,\end{aligned} \tag{B.24}$$

since $F_2(l_1,l_2,m_1,m_2,\tau) = -F_1(l_1,l_2,m_1,m_2,\tau)$.

Equations (B.23) and (B.24) give the form of the differential operator in (B.17). For example, the first two terms are given by

$$c_1^{0,0}(\mathbf{l}) = -\frac{l_2}{l_1^2+l_2^2}, \tag{B.25}$$

$$c_1^{0,1}(\mathbf{l}) = \frac{l_1^2-l_2^2}{(l_1^2-l_2^2)^2} \quad \text{and} \quad c_1^{1,0}(\mathbf{l}) = -\frac{2l_1l_2}{(l_1^2+l_2^2)^2}. \tag{B.26}$$

Now, we use the formulae (B.23), (B.24) in the expansion (B.22) for $I$ to get

$$I_j = \sum_{n=0}^{\infty}\frac{\tau^n}{n!}\sum_{\substack{r,q\\ r+q=n}} c_j^{r,q}(\mathbf{l})\frac{i}{(2\pi)^2}\int\int_{\mathbf{R}^2\setminus B} m_1^r m_2^q\hat{\omega}(\mathbf{m})dm_1dm_2, \tag{B.27}$$

where $j = 1,2$ identifies the component. We want to identify the moments of $\hat{\omega}$ (in (B.27)) with derivatives of $\omega$. To do this however, we need to extend the region of integration to all $\mathbf{R}^2$. We must also analyze the error in doing this. Write,

$$\begin{aligned}&\frac{i}{(2\pi)^2}\int\int_{\mathbf{R}^2\setminus B} m_1^r m_2^q\hat{\omega}(\mathbf{m})dm_1dm_2 \\ &\quad= \frac{i}{(2\pi)^2}\int\int_{\mathbf{R}^2} m_1^r m_2^q\hat{\omega}(\mathbf{m})dm_1dm_2 - \frac{i}{(2\pi)^2}\int\int_B m_1^r m_2^q\hat{\omega}(\mathbf{m})dm_1dm_2 \\ &\quad= i^{1-r-q}[\partial_x^r\partial_y^q\omega](\mathbf{0}) - \frac{i}{(2\pi)^2}\int\int_B m_1^r m_2^q\hat{\omega}(\mathbf{m})dm_1dm_2.\end{aligned} \tag{B.28}$$

The error term (the second term of (B.28)) can be seen to be of arbitrary order since $\mathbf{l}\in\Lambda^*(\alpha_1,\alpha_2)\setminus\mathbf{0}$. This is shown as follows: Since $|\hat{\omega}(\mathbf{m})| \le \frac{c}{|\mathbf{m}|^M}$ for any $M$ with $|\mathbf{m}|$ sufficiently large (because $\omega$ is smooth), we get

$$\begin{aligned}E \equiv \Big|\int\int_B m_1^r m_2^q\hat{\omega}(\mathbf{m})dm_1dm_2\Big| &\le c\int\int_B |\mathbf{m}|^n\frac{1}{|\mathbf{m}|^M}dm_1dm_2 \\ &\le c\int\int_B |\mathbf{m}|^{n-M}dm_1dm_2 \\ &\le c\tau^{M-n}\int_-^+\int_-^+\frac{d\tilde{m}_1d\tilde{m}_2}{[(\tau\tilde{m}_1+l_1)^2+(\tau\tilde{m}_2+l_2)^2]^{\frac{M-n}{2}}}\end{aligned} \tag{B.29}$$

by changing variables. Now, let us suppose that $\mathbf{l} = (l_1, l_2) \in \Lambda^*(\alpha_1, \alpha_2)\backslash\mathbf{0}$. Then, we can choose $\tau(= \frac{h}{2\pi})$ small enough

$$\tau < \tfrac{1}{4}\min(1/\alpha_1, 1/\alpha_2), \tag{B.30}$$

so that there is no singularity in the integrand of (B.29), and obtain the bound

$$E \le c\frac{(2\tau)^{M-n}}{(l_1^2 + l_2^2)^{\frac{M-n}{2}}}. \tag{B.31}$$

As this is true for any $M$, this term is of arbitrary order. Therefore, combining (B.27), (B.28), (B.31), we get

$$I_j = \sum_{n=0}^{N-1} \frac{\tau^n}{n!} \sum_{\substack{r,q \\ r+q=n}} c_j^{r,q}(\mathbf{l}) i^{1-r-q} [\partial_x^r \partial_y^q \omega](\mathbf{0}) + O\left(\frac{\tau^N}{|l|^N}\right) \tag{B.32}$$

for any $N$ and $\mathbf{l} \in \Lambda^*(\alpha_1, \alpha_2)\backslash\mathbf{0}$. This takes care of the first term in (B.21).

It now remains to consider the second term.

$$II = \frac{i}{(2\pi)^2} \int\int_B \mathbf{F}(l_1, l_2, m_1, m_2, \tau)\hat{\omega}(\mathbf{m}) dm_1 dm_2. \tag{B.33}$$

This term is also seen to be of arbitrary order.

Without loss of generality, we consider the case with $F_1$. We have

$$II_1 = \frac{i}{(2\pi)^2} \int\int_B F_1(l_1, l_2, m_1, m_2, \tau)\hat{\omega}(\mathbf{m}) dm_1 dm_2. \tag{B.34}$$

By changing variables and using again that $|\hat{\omega}(m)| \le \frac{c}{|\mathbf{m}|^M}$, for any $M$, we obtain

$$|II_1| \le c\tau^{-2} \int_{-\tau}^{+\tau} \int_{-\tau}^{+\tau} \frac{|\tilde{m}_2|}{\tilde{m}_1^2 + \tilde{m}_2^2} \frac{d\tilde{m}_1 d\tilde{m}_2}{\left[\left(\frac{\tilde{m}_2 + l_2}{\tau}\right)^2 + \left(\frac{\tilde{m}_1 + l_1}{\tau}\right)^2\right]^{\frac{M}{2}}}. \tag{B.35}$$

Now, if $\mathbf{l} \in \Lambda^*(\alpha_1, \alpha_2)\backslash\mathbf{0}$ and $\tau$ satisfies (B.30), then the only singularity of the integrand is due to the term $1/(\tilde{m}_1^2 + \tilde{m}_2^2)$, which is integrable. Consequently, we have

$$|II_1| \le c\frac{(2\tau)^{M-1}}{(l_1^2 + l_2^2)^{M/2}}, \tag{B.36}$$

and thus this term is also of arbitrary order.

Now, combining the results, (B.14), (B.21), (B.32), and (B.36), we get the result

(B.37)

$$\text{P.V.} \sum_{l_j \in \Lambda^*(\alpha_1,\alpha_2)\backslash\mathbf{0}} (\widehat{\mathbf{K}\omega})_m \left(\frac{1}{\tau}\mathbf{l_j}\right) = -\sum_{n=0}^{N-1} \frac{\tau^{n+1}}{n!} \lim_{\epsilon \to o} \sum_{l_j \in \Lambda^*(\alpha_1,\alpha_2)\backslash\mathbf{0}} \hat{\delta}_\epsilon \left(\frac{1}{\tau}\mathbf{l_j}\right) \cdot \sum_{\substack{r,q \\ r+q=n}} c_m^{r,q}(\mathbf{l_j}) i^{1-r-q} [\partial_x^r \partial_y^q \omega](\mathbf{0}) + O(\tau^{N+1})$$

for any $N$ sufficiently large, and where $m = 1, 2$ denotes the component.

Finally, the $n = 0$ term, all the terms even in $n$, and parts of the odd terms vanish due to oddness of the summands in the lattice sum. (See (B.25), (B.26) for example.) Therefore, identifying $\tau = h/2\pi$ and the surviving terms with $\tilde{\mathbf{C}}(\alpha)[\omega]$ yields the result (B.16), and thus completes the proof of the Fourier lattice sum expansion lemma. This lemma, combined with the self-induction term, proves the result (A.6) and completes the proof of the point vortex error expansion.

**Appendix C. Calculating the Second-Order Coefficient.** In this appendix, we derive the expression in (2.8) for the second-order error coefficient $C[\omega]_{j,2}$. Although the value of the second-order term is independent of the choice of smoothing function used, the ease with which it can be actually computed depends very much on this choice. The higher-order coefficients present no such difficulty as their associated lattice sums converge absolutely and can thus be calculated (if necessary) in a straightforward manner.

We begin with some notation. Define the lattice sum by

$$S(\alpha) = 4\sum_{m=1}^{\infty} \frac{1}{m}[f(m;\alpha)], \tag{C.1}$$

where

$$f(m;\alpha) = \frac{1}{m}\sum_{l=0}^{m}{}' \left[\frac{(l/m)^2 - \alpha^2}{[(l/m)^2+\alpha^2]^2} + \frac{1-\alpha^2(l/m)^2}{[1+\alpha^2(l/m)^2]^2}\right], \tag{C.2}$$

and $\sum'$ denotes the trapezoidal sum(i.e., the endpoints are weighted by $\frac{1}{2}$). The purpose of this appendix is to prove the following result given in §2.

THEOREM. SECOND-ORDER ERROR COEFFICENT. *For $\omega(\mathbf{x})$ smooth and rapidly decaying, the second-order error coefficient can be given as*

$$\mathbf{C}[\omega]_{\mathbf{j},2}h^2 = \frac{1}{4\pi}(-\omega_y(\mathbf{x_j})C_2(\alpha), \omega_x(\mathbf{x_j})C_2(1/\alpha))h_1h_2, \tag{C.3}$$

*where $h_1 = \alpha_1 h$, $h_2 = \alpha_2 h$, $\alpha$ is the grid aspect ratio $\alpha_1/\alpha_2$, and*

$$C_2(\alpha) = \frac{4}{\pi}\arctan(1/\alpha) - \frac{\alpha}{\pi}S(\alpha). \tag{C.4}$$

*Remark* 1. In the special case of a square grid $\alpha = 1$, we have $S(1) = 0$ and the second-order term then has the form

$$\mathbf{C}[\omega]_{\mathbf{j},2}h^2 = \frac{1}{4\pi}\nabla^{\perp}\omega(\mathbf{x_j})h_1h_2,$$

where $\nabla^{\perp}\omega = (-\omega_{x_2}, \omega_{x_1})$.

*Remark* 2. In the analysis of Goodman, Hou, and Lowengrub [16], it is essentially the smoothing function that gives rise to the undetermined constant of integration appearing in their second-order coefficient. We determine it explicitly.

*Proof.* Without loss of generality, we consider the case $\mathbf{x}_j = \mathbf{0}$. From (B.6), (B.9), (B.14), (B.26), and (B.27) $\mathbf{C}[\omega]_{\mathbf{0},2}$ can be given as

(C.5)

$$\mathbf{C}[\omega]_{\mathbf{0},2}h^2 = \lim_{\epsilon\to 0}(\mathbf{K}w)_\epsilon(\mathbf{0})h_1h_2 - \nabla^{\perp}w(\mathbf{0})\left(\frac{h}{2\pi}\right)^2 \lim_{\epsilon\to 0}\sum_{\mathbf{l}\in\Lambda^*(\alpha_1,\alpha_2)\setminus\mathbf{0}} \frac{l_1^2 - l_2^2}{|\mathbf{l}|^4}\hat{\delta}_\epsilon\left(\frac{2\pi}{h}\mathbf{l}\right),$$

where $\mathbf{l} = (l_1, l_2)$ and $h_1 = \alpha_1 h, h_2 = \alpha_2 h$.

The two terms to be considered are the self-induction term

$$\lim_{\epsilon \to 0} (\mathbf{K}\omega)_\epsilon(\mathbf{0}) \tag{C.6}$$

and the lattice sum

$$\lim_{\epsilon \to 0} \sum_{\mathbf{l} \in \Lambda^*(\alpha_1, \alpha_2) \setminus \mathbf{0}} \frac{l_1^2 - l_2^2}{(l_1^2 + l_2^2)^2} \hat{\delta}_\epsilon \left( \frac{2\pi}{h} \mathbf{l} \right). \tag{C.7}$$

Setting $\epsilon = 0$ in (C.7) gives a sum that is only conditionally convergent, and whose value depends upon how it is summed. The specific summation rule is dictated by $\hat{\delta}_\epsilon$. Here, we choose a sharp square cutoff. Let $\epsilon = \frac{1}{M}$ and

$$\hat{\delta}_{\frac{1}{M}} \left( \frac{2\pi}{h} \mathbf{l} \right) = \begin{cases} 1 \text{ if } |l_1| \le \dfrac{M}{\alpha_1} \text{ and } |l_2| \le \dfrac{M}{\alpha_2}, \\ 0 \text{ otherwise.} \end{cases} \tag{C.8a}$$

This in turn gives the Dirichlet kernel

$$\delta_{\frac{1}{M}}(x_1, x_2) = \frac{1}{\pi^2} \frac{\sin\left(\dfrac{M x_1}{\alpha_1}\right)}{x_1} \frac{\sin\left(\dfrac{M x_2}{\alpha_2}\right)}{x_2}. \tag{C.8b}$$

Now, using (C.8a) in (C.7) gives the lattice sum

$$\alpha \alpha_1 \alpha_2 \lim_{M \to \infty} \sum_{l_1 = -M}^{+M} \sum_{\substack{l_2 = -M \\ l \neq 0}}^{+M} \frac{l_1^2 - \alpha^2 l_2^2}{(l_1^2 + \alpha^2 l_2^2)^2}, \tag{C.9}$$

and using (C.8b) in (C.6) yields

$$\begin{aligned} &\lim_{M \to \infty} (\mathbf{K}\omega)_{\frac{1}{M}}(\mathbf{0}) \\ &\qquad = \frac{1}{\pi^2} \lim_{M \to \infty} \int\int_{\mathbf{R}^2} \mathbf{K}(\mathbf{x}) \omega(\mathbf{x}) \frac{\sin(M x_1/\alpha_1)}{x_1} \frac{\sin(M x_2/\alpha_2)}{x_2} dx_1 dx_2. \end{aligned} \tag{C.10}$$

Thus, we need to determine (C.9) and (C.10). We begin with the self-induction term (C.10).

SELF-INDUCTION LEMMA. *For $\omega(\mathbf{x})$ smooth and rapidly decaying, the self-induction term is given by*

$$\lim_{M \to \infty} (\mathbf{K}\omega)_{\frac{1}{M}}(\mathbf{0}) = \frac{1}{\pi^2} \left( -\omega_{x_2}(\mathbf{0}) \arctan\left(\frac{1}{\alpha}\right), \omega_{x_1}(\mathbf{0}) \arctan(\alpha) \right). \tag{C.11}$$

*Proof.* Apply (A.19) with $f = K_i \omega$, where $i = 1, 2$ denotes the component of $\mathbf{K}$. In light of (A.18), (A.20)–(A.22), and (A.28), it is clear that the proof reduces to evaluating

$$\begin{aligned} \lim_{M \to \infty} (K_i \omega)_{\frac{1}{M}}(\mathbf{0}) &= \lim_{M \to \infty} \frac{1}{\pi^2} \nabla \omega(\mathbf{0}) \\ &\cdot \int_{\frac{-RM}{\alpha_1}}^{\frac{+RM}{\alpha_1}} \int_{\frac{-RM}{\alpha_2}}^{\frac{+RM}{\alpha_2}} \tilde{\mathbf{H}}_i(\alpha_1 x_1, \alpha_2 x_2) \frac{\sin(x_1)}{x_1} \frac{\sin(x_2)}{x_2} dx_2 dx_1, \end{aligned} \tag{C.12}$$

where $\tilde{\mathbf{H}}_i(\mathbf{x}) = \mathbf{x}K_i(\mathbf{x})$. Without loss of generality, take $i = 2$. Then, (C.12) reduces to (C.13)

$$\lim_{M\to\infty}(K_2\omega)_{\frac{1}{M}}(\mathbf{0}) = \frac{\omega_{x_1}(\mathbf{0})}{\pi^2}\lim_{M\to\infty}\int_{\frac{-RM}{\alpha_1}}^{\frac{+RM}{\alpha_1}}\int_{\frac{-RM}{\alpha_2}}^{\frac{+RM}{\alpha_2}}\frac{x_1^2}{x_1^2+\left(\frac{x_2}{\alpha}\right)^2}\frac{\sin(x_2)}{x_2}\frac{\sin(x_1)}{x_1}dx_2dx_1,$$

where $\alpha = \alpha_1/\alpha_2$ is the grid aspect ratio. The term involving $\omega_{x_2}$ vanishes due to oddness of the integrand in each coordinate direction. With some care, the inner integral can be evaluated by contour integration. In particular, the regions of integration of both the inner and outer integrals must be divided appropriately so that the contour integration is justified. We do not present the details here. The $K_1$ integral is evaluated similarly. It now remains to consider the lattice sum (C.9). We obtain the following result.

LATTICE SUM LEMMA. *The sum in* (C.9), *omitting the* $\alpha\alpha_1\alpha_2$ *prefactor, is given by* (i)

$$S(\alpha) = \lim_{M\to\infty}\sum_{l_1=-M}^{+M}\sum_{\substack{l_2=-M\\ l\neq o}}^{+M}\frac{l_1^2-\alpha^2l_2^2}{(l_1^2+\alpha^2l_2^2)^2} = 4\sum_{m=1}^{\infty}\frac{1}{m}f(m;\alpha), \tag{C.14}$$

*where*

$$f(m;\alpha) = \frac{1}{m}{\sum_{k=0}^{m}}'\left[\frac{(k/m)^2-\alpha^2}{[(k/m)^2+\alpha^2]^2}+\frac{1-\alpha^2(k/m)^2}{[1+\alpha^2(k/m)^2]^2}\right], \tag{C.15}$$

*where* $\sum'$ *denotes the trapezoidal sum* (*i.e., the endpoints are weighted by* $\frac{1}{2}$). *For* $m \gg 1$, *we have* (ii)

$$\begin{aligned} f(m;\alpha) &= \frac{1}{6}\frac{\alpha^2-1}{(1+\alpha^2)^2}\frac{1}{m^2} - \frac{1}{30}\frac{(\alpha^2-1)(\alpha^4-10\alpha^2+1)}{(1+\alpha^2)^4}\frac{1}{m^4} + O\left(\frac{1}{m^6}\right) \\ &\equiv f_2(\alpha)\frac{1}{m^2} + f_4(\alpha)\frac{1}{m^4} + O\left(\frac{1}{m^6}\right). \end{aligned} \tag{C.16}$$

*Proof of Lemma.* (i) Using the four-fold symmetry of the summand over quadrants, we rewrite the sum (C.9) as

$$S(\alpha) = \lim_{M\to\infty}\sum_{l_1=-M}^{+M}\sum_{\substack{l_2=-M\\ l\neq 0}}^{+M}\frac{l_1^2-\alpha^2l_2^2}{(l_1^2+\alpha^2l_2^2)^2} = \lim_{M\to\infty}4{\sum_{l_1=0}^{M}}''{\sum_{\substack{l_2=0\\ l\neq 0}}^{M}}''\frac{l_1^2-\alpha^2l_2^2}{(l_1^2+\alpha^2l_2^2)^2}, \tag{C.17}$$

where $\sum''$ denotes that terms with $l_1 = 0$ or $l_2 = 0$ are weighted by $\frac{1}{2}$. Then, by summing first out along the diagonal of the lattice, we get

$$S(\alpha) = \lim_{M\to\infty}4\sum_{m=1}^{M}{\sum_{k=0}^{m}}'\left[\frac{k^2-\alpha^2m^2}{(k^2+\alpha^2m^2)^2}+\frac{m^2-\alpha^2k^2}{(m^2+\alpha^2k^2)^2}\right], \tag{C.18}$$

$$= \lim_{M\to\infty}4\sum_{m=1}^{M}\frac{1}{m}\left[\frac{1}{m}{\sum_{k=0}^{m}}'\frac{(k/m)^2-\alpha^2}{((k/m)^2+\alpha^2)^2}+\frac{(1-\alpha^2(k/m)^2)^2}{(1+\alpha^2(k/m)^2)^2}\right], \tag{C.19}$$

$$= 4 \sum_{m=1}^{\infty} \frac{1}{m} f(m;\alpha), \tag{C.20}$$

which gives the result (i).

The self-induction lemma and result (i) of the lattice sum lemma together give the second-order error coefficient in (C.3) and (C.4), and completes the proof of the theorem. We now consider result (ii) of the lattice sum lemma, which gives the large $m$ asymptotics of $f$ and leads to our rapid summation corollary.

The function $f(m;\alpha)$, (C.15), is the trapezoidal rule approximation of the integrals

$$\int_0^1 \frac{x^2-\alpha^2}{(x^2+\alpha^2)^2} dx + \int_0^1 \frac{1-\alpha^2 x^2}{(1+\alpha^2 x^2)^2} dx. \tag{C.21}$$

Thus, $f(m;\alpha)$ can be written as

$$f(m;\alpha) = \int_0^1 \frac{x^2-\alpha^2}{(x^2+\alpha^2)^2} dx + \int_0^1 \frac{1-\alpha^2 x^2}{(1+\alpha^2 x^2)^2} dx + E_1(m;\alpha) + E_2(m;\alpha), \tag{C.22}$$

where the errors $E_1$ and $E_2$ are given by

$$E_1(m;\alpha) = \frac{1}{m} {\sum_{k=0}^{m}}' \frac{(k/m)^2-\alpha^2}{((k/m)^2+\alpha^2)^2} - \int_0^1 \frac{x^2-\alpha^2}{(x^2+\alpha^2)^2} dx \tag{C.23}$$

and

$$E_2(m;\alpha) = \frac{1}{m} {\sum_{k=0}^{m}}' \frac{1-\alpha^2(k/m)^2}{(1+\alpha^2(k/m)^2)^2} - \int_0^1 \frac{1-\alpha^2 x^2}{(1+\alpha^2 x^2)^2} dx. \tag{C.24}$$

Now, by direct calculation,

$$\int_0^1 \frac{x^2-\alpha^2}{(x^2+\alpha^2)^2} dx + \int_0^1 \frac{1-\alpha^2 x^2}{(1+\alpha^2 x^2)^2} dx = 0. \tag{C.25}$$

And, for $m \gg 1$, the error terms can be found through the Euler–MacLaurin expansion. This gives the result (ii).

We can now rapidly and accurately sum $S(\alpha)$ using the asymptotic form of $f$. In particular, we obtain the following corollary.

RAPID SUMMATION COROLLARY. *The sum $S(\alpha)$ can be rewritten so as to converge like $O(1/m^7)$ by using the expansion* (ii) *in the following way*:

$$S(\alpha) = \sum_{m=1}^{\infty} \frac{1}{m} \left[ f(m;\alpha) - f_2(\alpha)\frac{1}{m^2} - f_4(\alpha)\frac{1}{m^4} \right] + f_2(\alpha)\zeta(3) + f_4(\alpha)\zeta(5), \tag{C.26}$$

*where*

$$\zeta(s) = \sum_{m=1}^{\infty} \frac{1}{m^s}, \qquad s > 1,$$

*is the Riemann–Zeta function. In particular,* $\zeta(3) = 1.202056903159594$ *and* $\zeta(5) = 1.036927755143370$.

**Acknowledgments.** We thank Chris Anderson, Jonathan Goodman, Tom Hou, Joe Keller, Omar Knio, and Vered Rom-Kedar for valuable discussions. We thank the referees for their careful examination of the paper and their useful comments. We especially thank one of the referees for noticing a problem with our original formulation of the Poisson summation formula for singular functions. MJS would also like to thank the Mathematics Department at UCLA, where some of the writing and work on this paper was done, for their hospitality. Likewise, JSL would like to thank the Courant Institute for their hospitality.

## REFERENCES

[1] C. ANDERSON, *A method of local corrections for computing the velocity field due to a distribution of vortex blobs*, J. Comput. Phys., 62 (1986), pp. 111–123.
[2] C. ANDERSON AND C. GREENGARD, *On vortex methods*, SIAM J. Numer. Anal., 22 (1985), pp. 413–440.
[3] G. BAKER AND M. SHELLEY, *On the connection between thin vortex layers and vortex sheets*, J. Fluid Mech., 215 (1990), pp. 161–194.
[4] J. T. BEALE, *A convergent* 3-D *vortex method with grid free stretching*, Math. Comp., 46 (1986), pp. 401–424.
[5] J. T. BEALE AND A. MAJDA, *High order accurate vortex methods with explicit velocity kernels*, J. Comput. Phys., 58 (1985), pp. 188–208.
[6] ———, *Vortex methods* II: *High order accuracy in* 2 *and* 3 *dimensions*, Math. Comp., 32 (1982), pp. 29–52.
[7] J. B. BELL, P. COLLELA, AND H. M. GLAZ, *A second order projection method for the incompressible Navier–Stokes equations*, J. Comput., Phys., 58 (1989), pp. 188–208.
[8] J. U. BRACKBILL, *Coordinate System Control: Adaptive Meshes*, in Numerical Grid Generation, J. F. Thompson, ed., Elsevier, Amsterdam, North-Holland, 1982.
[9] J. BUNTINE AND D. I. PULLIN, *Merger and cancellation of strained vortices*, J. Fluid Mech., 205 (1989), p. 1632.
[10] A. J. CHORIN, *A numerical study of slightly viscous flow*, J. Fluid Mech., 57 (1973), pp. 785–796.
[11] P. COLLELA AND P. WOODWARD, *The piecewise parabolic method*, J. Comput. Phys., 54 (1984), p. 174.
[12] G. H. COTTET, *Methodes Particularies pour l'Equation d'Euler dans le Plan*, Thèse 3eme Cycle, Univ. Pierre et Marie Curie, Paris, France, 1982.
[13] G. H. COTTET, J. GOODMAN, AND T. Y. HOU, *Convergence of the grid-free point vortex method for the three-dimensional Euler equations*, SIAM J. Numer. Anal., 28 (1991), pp. 291–307.
[14] H. DYM AND H. P. MCKEAN, *Fourier Series and Integrals*, Academic Press, New York, 1972.
[15] D. FISHELOV, *A new vortex scheme for viscous flow*, J. Comput. Phys., 26 (1990), p. 399.
[16] J. GOODMAN, T. Y. HOU, AND J. LOWENGRUB, *Convergence of the point vortex method for the* 2-D *Euler equations*, Comm. Pure Appl. Math., 43 (1990), pp. 415–430.
[17] L. GREENGARD AND V. ROKHLIN, *A fast algorithm for particle summations*, J. Comput. Phys., 73 (1987), pp. 325–348.
[18] O. HALD, *Convergence of vortex methods* II, SIAM J. Numer. Anal., 16 (1979), pp. 726–755.
[19] A. HARTEN AND S. OSHER, *Uniformly high order accurate non-oscillatory schemes*, I, SIAM J. Numer. Anal., 24 (1987), pp. 279–309.
[20] T. Y. HOU, J. LOWENGRUB, AND M. J. SHELLEY, *The convergence of an exact desingularization and local regridding for vortex methods*, SIAM J. Sci. Comput., 14 (1993), pp. 1–18.
[21] J. LOWENGRUB AND M. J. SHELLEY, *Smooth Grid Methods for Vorticity Formulation of the Euler Equations*, in Vortex Dynamics and Methods, C. Anderson and C. Greengard, eds., Lectures in Applied Mathematics 18, American Mathematical Society, Providence, RI, 1991.
[22] R. B. PAYNE, *Calculations of unsteady viscous flow past a circular cylinder*, J. Fluid Mech., 4 (1958), pp. 81–86.
[23] R. PEYRET AND T. TAYLOR, *Computational Methods for Fluid Flow*, Springer Series in Computational Physics, Springer-Verlag, Berlin, New York, 1983.
[24] P. A. RAVIART, *An Analysis of Particle Methods*, in Numerical Methods in Fluid Dynamics, Lecture Notes in Math. 1127, Springer-Verlag, Berlin, New York, 1985, p. 243.
[25] V. ROM-KEDAR AND M. J. SHELLEY, *The dynamics of plumes in continuously stratified fluids*, manuscript.
[26] L. ROSENHEAD, *The point vortex approximation of a vortex sheet*, Proc. Roy. Soc. London Ser. A, 134 (1932), pp. 170–192.
[27] M. J. SHELLEY, D. MEIRON, AND S. ORSZAG, *Dynamical aspects of vortex reconnection of perturbed anti-parallel vortex tubes*, J. Fluid Mech., 246 (1993), p. 613.

[28] M. J. SHELLEY, *A study of singularity formation in vortex sheet motion by a spectrally accurate vortex method*, J. Fluid Mech., 244 (1992), p. 493.

[29] A. SIDI AND M. ISRAELI, *Quadrature methods for singular and weakly Fredholm integral equations*, J. Sci. Comput., 3 (1988), pp. 201–231.

[30] E. M. STEIN AND G. WEISS, *Introduction to Fourier Analysis on Euclidean Spaces*, Princeton University Press, Princeton, NJ, 1971.

[31] J. STOER AND R. BURLIRSCH, *Introduction to Numerical Analysis*, Springer-Verlag, Berlin, New York, 1980.